AD-A067 510 SCIENCE APPLICATIONS INC MCLEAN VA OCEAN SCIENCE DIV F/G 8/10
A NUMERICAL MODEL OF THE TROPICAL MARINE BOUNDARY LAYER FOR ASS--ETC(U)
MAR 78 R M CLANCY N00173-77-C-0033
UNCLASSIFIED SAI-79-748-WA NL

1 OF 2
ADA 067510

OF
A
5 | 0

LEVEL II C

AD A067510

(6) A NUMERICAL MODEL OF THE TROPICAL MARINE BOUNDARY LAYER FOR ASSESSING THE ENVIRONMENTAL IMPACT OF OCEAN THERMAL POWER PLANTS

(14) SAI-79-748-WA

(10) R. Michael Clancy
~~Fluid Mechanics Group~~
Ocean Science Division
Science Applications, Inc.
McLean, Virginia

(15) N00173-77-C-0033

(11) 31 March 1978

(12) 100p.

411104

63

ACKNOWLEDGMENT

The author would like to express his thanks to Dr. Steve Piacsek, Dr. Glyn Roberts, and Dr. Walter Grabowski for helpful suggestions regarding this work. He would also like to thank Ms. Barbara Czika for preparing the manuscript.

This work was largely supported by ERDA (now DOE) under contract E(49-26) 1005, monitored by Dr. L. F. Lewis. Our involvement in this contract was through Navy Contract N00173-77-C-0033.

TABLE OF CONTENTS

TABLE OF CONTENTS
(continued)

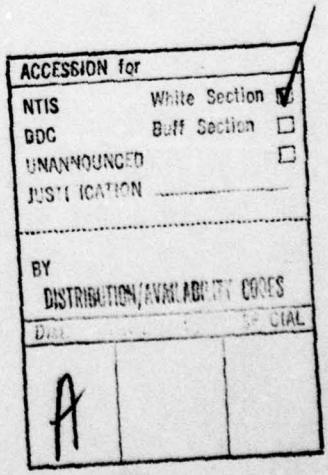

LIST OF TABLES AND FIGURES

LIST OF TABLES AND FIGURES
(continued)

ABSTRACT

A one-dimensional model of the tropical atmosphere consisting of conservation equations for heat, moisture, momentum and mass is constructed and used to investigate the effect of sea surface temperature perturbations on the local thermodynamic characteristics of the marine boundary layer in the summertime Western Atlantic trade wind regime.

The height of the trade wind inversion and the thickness of the atmospheric mixed layer are found to be little affected by changes of sea surface temperature in the range that would be produced by Ocean Thermal Power Plants. The surface fluxes of long-wave radiation, short-wave radiation, and sensible heat are practically unaffected by these small changes in the sea surface temperature or by changes in the intensity of the cumulus convection. The surface latent heat flux (taken positive downward), however, varies linearly with the sea surface temperature ~~with a slope of about -105 cal cm^{-2} day^{-1} °K^{-1}~~ and is strongly coupled to the intensity of the cumulus convection.

If the maximum tolerable change in the surface evaporation rate is taken to be at -5%, the maximum allowable OTPP-generated sea surface temperature perturbation is about -0.2°C.

Section 1

INTRODUCTION

The operation of one or more Ocean Thermal Power Plants (OTPP's) in a particular region will cool the upper layer of the ocean and reduce the sea surface temperature (SST) by, perhaps, as much as 1.5°C (Piacsek, et al., 1976). This will alter the net surface heat flux, E_o, the local thermodynamic structure of the atmosphere, and possibly the climate of the region downwind.

It is important to assess these environmental impacts before large numbers of OTPP's are put into operation. This point is underscored by the work of Shukla (1975) who performed experiments with a general circulation model and found that an average SST anomaly of -1.5°C in the Arabian Sea (over a region roughly the size of the Gulf of Mexico) reduced the model Monsoon rainfall in India by about 50%. This relationship between SST and rainfall was qualitatively supported by Shukla and Misra (1977) who analyzed 60 years of SST, wind speed, and rainfall data for that region. Such evidence linking rainfall to SST is disturbing since the Gulf of Mexico, which is the source region for most of the summertime rainfall in the mid-western United States, is also a proposed OTPP site.

In addition, Wendland (1977) analyzed nine years of SST and tropical storm frequency data for the Atlantic and found that decreases in SST of a few tenths of a degree Celsius over regions with areal extent of order 10^6 km^2, were associated with a significant decrease in the number of

monthly storms and the length of the storm season. Wendland's findings imply that large numbers of OTPP's operating in the Caribbean may decrease the tropical storm activity there. Since a significant percentage of the annual rainfall in the southeastern United States is due to tropical storms, it is not clear whether this would be desirable.

To ensure that OTPP's are deployed in such a manner that the environmental changes they cause fall within an acceptable range, it is necessary to determine the change in the net surface heat flux with respect to sea surface temperature, dE_o/dT_o. Piacsek et al. (1976) and Bathen et al. (1976) used bulk aerodynamic formulation and local meteorological data to estimate dE_o/dT_o at proposed OTPP sites near Puerto Rico and Hawaii, respectively. With this type of approach, however, it is necessary to make arbitrary assumptions about the atmosphere's thermodynamic adjustment to the SST perturbation. Another possible way of estimating dE_o/dT_o is to compare direct measurements of the surface fluxes at a particular location at another time of the year to those made at the same location at a different time of the year when the SST is different (summer and winter, for example). However, the large-scale flow patterns of the atmosphere's general circulation system also vary with the season and this would alter the seasonally-averaged surface fluxes whether the SST changes or not. Consequently, there would be no way to identify how much of the observed change in E_o was due purely to the change in SST. A more reliable approach is to explicitly model the atmospheric response to changes in SST.

A rather sophisticated model is necessary for this type of study since it must be capable of reproducing the observed average structure of the tropical marine boundary layer. This structure has been detailed by Garstang and Betts (1974) for the undisturbed (i.e., fair-weather) trade wind regime and consists essentially of (see Figure 1):

- A surface or "constant flux" layer extending from the sea surface to typically 50 m height in which potential temperature and water vapor mixing ratio decrease with altitude;
- A subcloud mixed layer extending from the top of the surface layer to roughly 500 m height in which potential temperature and water vapor mixing ratio are approximately constant with altitude;
- A thin transition layer at the top of the mixed layer in which potential temperature increases and water vapor mixing ratio decreases sharply with altitude; and
- A conditionally unstable cloud layer extending from the top of the transition layer to about 1-2 km height.

The marine boundary layer is topped by the trade inversion in which potential temperature increases and water vapor mixing ratio decreases rapidly with altitude. Below the transition layer the vertical eddy fluxes of heat and moisture are due mainly to dry convection and mechanical mixing, while above it these fluxes are accomplished primarily by cumulus convection. Thus, both dry convection

and cumulus convection provide important coupling mechanisms between the sea surface and the upper part of the marine boundary layer.

Recently a number of diagnostic studies have been carried out which clarify the role of cumulus convection in maintaining the thermodynamic structure of the tropical atmosphere. In these studies a model of the cumulus ensemble is used along with observed large-scale budgets of heat and moisture to deduce the characteristics of the clouds and their effect on the environment. This method was first applied to the undisturbed trade wind regime by Nitta (1975), who used a model fundamentally similar to that of Arakawa (1971) to analyze the BOMEX Phase III data. He found that most of the clouds were confined to below the trade inversion and that the large observed heat sink and moisture source in and near the base of the inversion was due primarily to the cooling and moistening effects of the detrainment of liquid water and saturated air from the clouds. These conclusions were also indicated by the work of Soong and Oqura (1976) who analyzed the same data set with a model consisting of six cloud types, each of which were simulated with a two-dimensional axisymmetric cloud model.

Representing the effects of cumulus clouds in a numerical prediction model is a difficult task. One way to accomplish this is to use a very high resolution three-dimensional model which explicitly resolves each individual member of the cumulus ensemble and simulates its full life cycle. This approach was taken by Sommeria (1975) in a remarkable paper. However, while this technique gives great insight into the relative importance of various

physical processes and clarifies the relationship between the cloud field and the subcloud layer turbulence field, it is practical only for very limited studies because of the tremendous computer resources required.

A more common approach to the problem is to parameterize the effects of cumulus clouds in terms of the model-predicted large-scale fields. This, of course, is intrinsically a more difficult task than the diagnostic determination of cumulus ensemble characteristics since it required prediction of both the characteristics of the ensemble and the time evolution of the large-scale fields. Cumulus parameterization has been one of the most important problems considered in tropical meteorology and has undergone rapid advances in recent years. Early attempts at cumulus parameterization consisted of simple convective adjustment schemes which conserved energy but did not explicitly take into account important processes such as compensating subsidence in the environment, entrainment and detrainment, and the re-evaporation of cloud droplets. The landmark paper of Arakawa and Schubert (1974) incorporated these processes into a spectral model of a cumulus ensemble and, for the first time, provided a closed and theoretically rigorous parameterization of the mutual interaction of a cumulus ensemble with the large-scale environment.

Modeling of the tropical subcloud mixed layer has also progressed rapidly in the past few years. Following the earlier work of Ball (1960) and Lilly (1968), Betts (1973) proposed a model which showed how the thermodynamic characteristics and the thickness of the mixed layer are controlled by large-scale mass convergence,

cloud-induced subsidence in the environment, and the radiative and surface fluxes. Ogura and Cho (1974) included the cloud-induced vertical eddy fluxes of heat and moisture at the top of the mixed layer into a model similar to that of the earlier studies. In all of these models, the transition layer is treated as a discontinuity in the thermodynamic variables at the top of the mixed layer. These studies are important in the present context because they indicate that the steady-state surface fluxes are determined by complex interactions involving the entire marine boundary layer.

Pond (1971,1972) reviewed surface layer models useful for predicting the surface fluxes in terms of mean field quantities. Since then a number of experiments have been performed which have increased our confidence in the empirical forms of the Monin-Obukhov similarity functions which arise in this type of treatment. Busch (1977) has given a comprehensive review of recent developments in this area.

A reliable determination of the atmospheric response to SST perturbations requires a comprehensive model which can realistically simulate the complex physical processes responsible for maintaining the structure of the marine boundary layer. Such a model has been constructed. The remainder of this paper will describe it, show some preliminary results, and indicate plans for future work.

Section 2

DESCRIPTION OF THE MODEL

2.1 FUNDAMENTAL EQUATIONS

Consider a region above the tropical ocean large enough to contain an ensemble of cumulus clouds but small enough to be regarded as a fraction of a large-scale system. Taking pressure as the vertical coordinate, the equations for conservation of heat, moisture, momentum and mass spatially averaged on constant pressure surfaces in the region can be written (Yanai, Esbensen, and Chu (1973))

$$\frac{\partial \bar{s}}{\partial t} + \bar{\underline{v}}\cdot\overline{\nabla s} + \bar{\omega}\frac{\partial \bar{s}}{\partial p} = \bar{Q}_R + L_v(\bar{c} - \bar{e}) - \frac{\partial}{\partial p}\overline{s'\omega'} \quad , \quad (1)$$

$$\frac{\partial \bar{q}}{\partial t} + \bar{\underline{v}}\cdot\overline{\nabla q} + \bar{\omega}\frac{\partial \bar{q}}{\partial p} = \bar{e} - \bar{c} - \frac{\partial}{\partial p}\overline{q'\omega'} \quad , \quad (2)$$

$$\frac{\partial \bar{u}}{\partial t} + \bar{\underline{v}}\cdot\overline{\nabla u} + \bar{\omega}\frac{\partial \bar{u}}{\partial p} = f(\bar{v} - \bar{v}_g) - \frac{\partial}{\partial p}\overline{u'\omega'} \quad , \quad (3)$$

$$\frac{\partial \bar{v}}{\partial t} + \bar{\underline{v}}\cdot\overline{\nabla v} + \bar{\omega}\frac{\partial \bar{v}}{\partial p} = f(\bar{u}_g - \bar{u}) - \frac{\partial}{\partial p}\overline{v'\omega'} \quad , \quad (4)$$

$$\nabla\cdot\bar{\underline{v}} + \frac{\partial \bar{\omega}}{\partial p} = 0 \quad , \quad (5)$$

where s is the dry static energy given by

$$s = c_p T + gz \quad , \quad (6)$$

q the mixing ratio of water vapor (mass of water vapor per mass of dry air), u the east-west component of wind speed, v the north-south component of wind speed, $\underline{v}$ the horizontal wind velocity vector, p the pressure, ω the vertical p-velocity $\omega = \frac{dp}{dt}$, Q_R the net radiational heating rate, c the rate of condensation per unit mass of air, and e the rate of evaporation per unit mass of air. Other symbols are defined in Appendix A and all of the notation is standard. Spatial averages at constant p taken across the entire model domain are denoted by $(\bar{})$, primes indicate departures from these averages, gradients taken at constant pressure are denoted by (∇), and we assume that fluctuations in the horizontal components of wind are uncorrelated with s′, q′, u′, and v′.

We also assume that the fraction of the model domain covered by active cumulus clouds, σ, is small. Thus, since s and q inside cumulus clouds over the tropical ocean are not observed to depart substantially from s and q of the environment, we have

$$\bar{s} \sim \tilde{s} \quad ,$$

$$\bar{q} \sim \tilde{q} \quad , \tag{7}$$

where $(\tilde{})$ denotes horizontal averages taken across the clear region between the clouds. Furthermore, from mass continuity, we have

$$\bar{\omega} = \bar{\omega}_\sigma + (1 - \sigma)\tilde{\omega} \sim \bar{\omega}_\sigma + \tilde{\omega} \quad , \tag{8}$$

with $\bar{\omega}_\sigma$ given by

$$\bar{\omega}_\sigma = \sum_{i=1}^{N} \omega_i \sigma_i \quad , \tag{9}$$

where ω_i is the average vertical p-velocity at a particular level inside the i-th cloud, σ_i is the fraction of the model domain covered by the i-th cloud, and N is the total number of clouds. Note that $\bar{\omega}_\sigma$ is observed to be large relative to $\bar{w}$. Thus, in general,

$$\bar{\omega} \neq \tilde{\omega} \quad .$$

In addition, we have the hydrostatic equation

$$\frac{\partial \bar{p}}{\partial z} = - \bar{\rho} g \quad , \tag{10}$$

the equation of state for moist air

$$\frac{p}{\rho} = RT(1 + 0.61q) \quad , \tag{11}$$

and the equation for potential temperature

$$\theta = T\left(\frac{p_o}{p}\right)^{R/c_p} \quad , \tag{12}$$

where ρ is the density of the moist air, g the acceleration of gravity, z the altitude, R the gas constant for dry air, p_o the surface pressure, T the temperature, and c_p the

specific heat at constant pressure for dry air. Note that since q is at most $0(10^{-2})$, we assume that the specific heat of moist air is given by the specific heat of dry air, which is common practice. This along with the assumed hydrostatic balance of the environment gives from (6) and (12)

$$\frac{\partial \bar{s}}{\partial z} = c_p\left(\frac{p}{p_o}\right)^{R/c_p} \frac{\partial \bar{\theta}}{\partial z} \quad . \tag{13}$$

Thus, a layer of constant potential temperature is also a layer of constant dry static energy.

The following six subsections give a comprehensive discussion of various simplifying assumptions applied to the basic model equations, the parameterizations used, and the numerical techniques employed. The reader who wishes only a summary of the resulting model formulation may skip to Section 2.8.

2.2 THE SUBCLOUD MIXED LAYER

2.2.1 Thermodynamic Equations

Consistent with the observations of Bunker et al. (1949), Malkus (1958), and many others, we assume that a mixed layer exists, extending from the top of the surface layer to a level denoted by p_b, in which s and q are constant with height. We denote the pressure at the top of the surface layer by p_a, the pressure at cloud base by p_c, and restrict our attention to the typical trade wind situation whre $p_a > p_b > p_c$ in all that follows.

We will model the subcloud mixed layer with the formulation of Arakawa and Schubert (1974). In this type of treatment the transition layer is modeled as a discontinuity in s and q at p_b. This is illustrated in Figure 1.

Defining s_m and q_m as the horizontally-averaged mixed layer values of dry static energy and water vapor mixing ratio, and assuming no condensation or evaporation of cloud droplets or raindrops occurs in the mixed layer, (1) and (2) can be integrated over the mixed layer depth to yield

$$\frac{\partial s_m}{\partial t} + \left(\bar{\underline{v}}\cdot\overline{\nabla s}_m\right)_M = \frac{\left|(\overline{\omega' s'})_b - (\overline{\omega' s'})_a\right|}{p_b - p_a} + \left(\bar{Q}_R\right)_M , \tag{14}$$

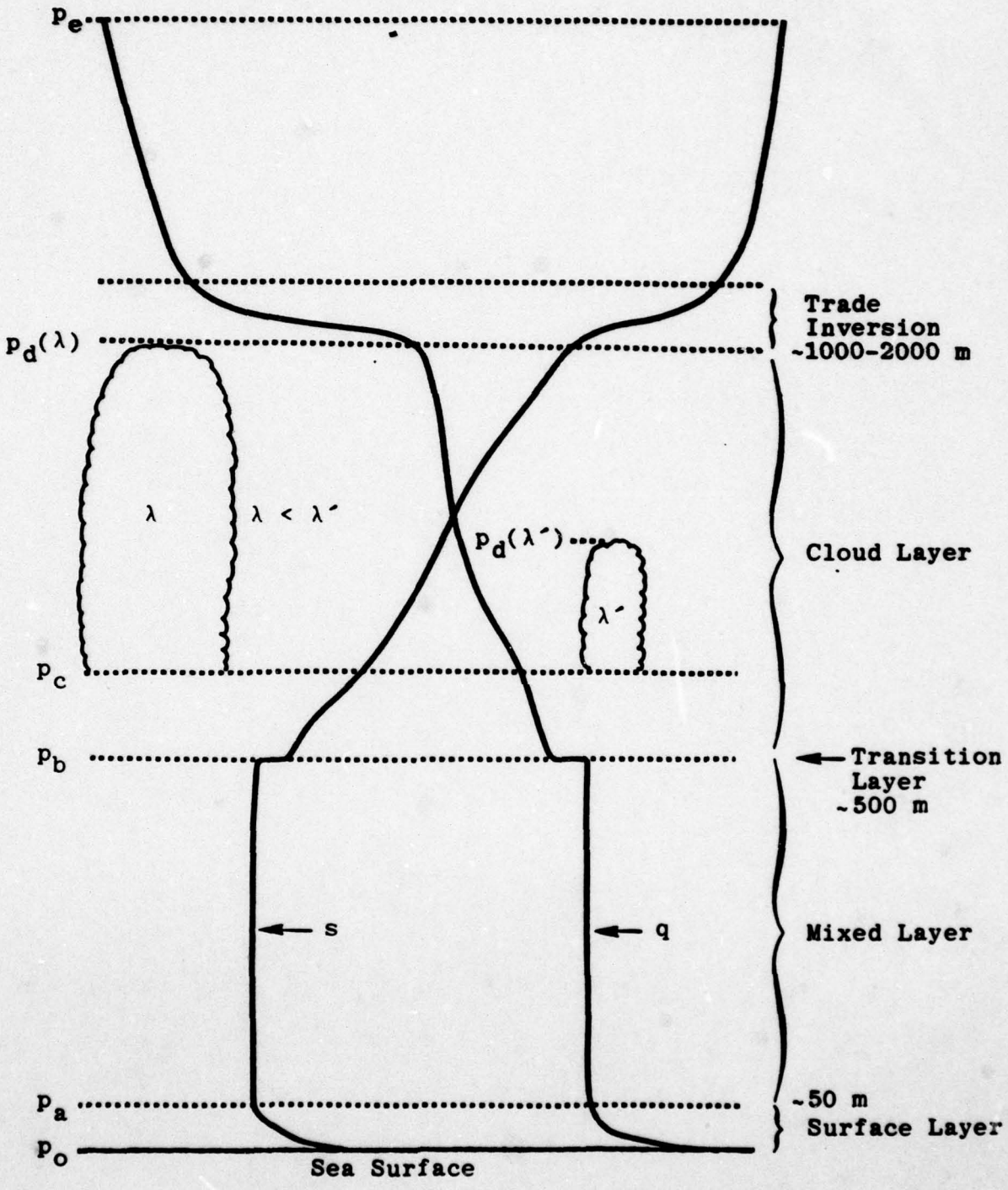

Figure 1. Schematic diagram of the basic model structure (not to scale). See text for discussion.

$$\frac{\partial q_m}{\partial t} + \overline{\underline{v}}\cdot\overline{\nabla q}_{m\,M} = \frac{\left|(\overline{\omega' q'})_b - (\overline{\omega' q'})_a\right|}{p_b - p_a} \quad , \qquad (15)$$

where

$$(\ )_M \equiv \frac{1}{p_b - p_a} \int_{p_a}^{p_b} (\ )\, dp \quad .$$

The terms $(\overline{\omega' s'})_b$ and $(\overline{\omega' q'})_b$ are the turbulent fluxes of s and q at the base of the transition layer. They arise because the turbulence at the top of the mixed layer due to dry convection entrains the generally warmer and dryer air above. As mentioned in Section 1, it is observed that the eddy fluxes due to dry convection are confined to below the top of the transition layer. Thus the entrainment fluxes go to zero at the top of the infinitely thin transition layer which is denoted by $p_{\overline{b}}$.

We now define

$$\Delta s \equiv \overline{s}(p_{\overline{b}}) - s_m \quad ,$$

$$\Delta q \equiv \overline{q}(p_{\overline{b}}) - q_m \quad , \qquad (16)$$

and consider the heat and moisture budgets in the transition layer. The total downward fluxes of s and q through the top of the transition layer in the region between the clouds are

$$(s_m + \Delta s) - \frac{\partial p_b}{\partial t} + \bar{\underline{v}}_b \cdot \overline{\nabla p}_b + \tilde{\omega}_b \quad ,$$

and

$$(q_m + \Delta q) - \frac{\partial p_b}{\partial t} + \bar{\underline{v}}_b \cdot \overline{\nabla p}_b + \tilde{\omega}_b \quad , \qquad (17)$$

while the downward fluxes of s and q through the bottom of the transition layer in the cloud-free region are

$$s_m \left[- \left(\frac{\partial p_b}{\partial t} + \bar{\underline{v}}_b \cdot \overline{\nabla p}_b \right) + \tilde{\omega}_b \right] + (\overline{\omega' s'})_b \quad ,$$

and

$$q_m \left[- \left(\frac{\partial p_b}{\partial t} + \bar{\underline{v}}_b \cdot \overline{\nabla p}_b \right) + \tilde{\omega}_b \right] + (\overline{\omega' q'})_b \quad , \qquad (18)$$

where $\tilde{\omega}_b$ is the average vertical p-velocity in the environment between the clouds at p_b. Combining (17) and (18) and requiring the fluxes of s and q to be continuous across the transition layer yields

$$\frac{\partial p_b}{\partial t} + \bar{\underline{v}}_b \cdot \overline{\nabla p}_b = \tilde{\omega}_b - \frac{(\overline{\omega' s'})_b}{\Delta s} \quad ,$$

$$\frac{\partial p_b}{\partial t} + \bar{\underline{v}}_b \cdot \overline{\nabla p}_b = \tilde{\omega}_b - \frac{(\overline{\omega' q'})_b}{\Delta q} \quad , \qquad (19)$$

which imply

$$(\overline{\omega' q'})_b = \frac{\Delta q}{\Delta s} (\overline{\omega' s'})_b \quad . \qquad (20)$$

The horizontally-averaged virtual dry static energy is given to excellent approximation by

$$\overline{s}_v = \overline{s} + 0.61\, c_p\, \overline{T}\, \overline{q} \quad , \tag{21}$$

where the term arising from the correlation of T' and q' has been neglected. The virtual dry static energy accounts for the effect of moisture on the buoyancy of an air parcel. Following Lilly (1968), Betts (1973), and others, we assume that the turbulent flux of virtual s at the top of the mixed layer can be written

$$\left(\overline{\omega' s_v'}\right)_b = - k\left(\overline{\omega' s_v'}\right)_o \quad , \tag{22}$$

where $\left(\overline{\omega' s_v'}\right)_o$ is the surface flux of s_v, given to excellent approximation by

$$\left(\overline{\omega' s_v'}\right)_o = (\overline{\omega' s'})_o + 0.61\, c_p\, \overline{T}(\overline{\omega' q'})_o \quad , \tag{23}$$

and k is a constant. Equation (22) arises from consideration of the turbulent energy balance in the mixed layer which requires k to be in the range of 0 to 1. Deardorff *et al*. (1969) suggested $k \cong 0.10$ from laboratory experiments, while Betts (1973) suggested $k \cong 0.25$.

Combination of (20) through (23) yields

$$(\overline{\omega' s'})_b = - \frac{k\Delta s}{\Delta s_v} \left(\overline{\omega' s_v'}\right)_o \quad ,$$

$$(\overline{\omega' q'})_b = - \frac{k\Delta q}{\Delta s_v} \left(\overline{\omega' s_v'}\right)_o \quad , \tag{24}$$

where

$$\Delta s_v = \Delta s + 0.61\, c_p\, \overline{T}\, \Delta q \quad . \tag{25}$$

In general, Δq is negative while Δs and Δs_v are positive. Note that $\Delta s_v > 0$ is required for dry convective stability at the top of the mixed layer.

Equations (8), (14), (15), (19), and (24) can be combined to yield

$$\frac{\partial s_m}{\partial t} = - \left(\overline{\underset{\sim}{v}} \cdot \overline{\nabla s}_m\right)_M - \frac{1}{p_a - p_b}\left[\left(\overline{\omega' s'}\right)_a + k\frac{\Delta s}{\Delta s_v}\left(\overline{\omega' s_v'}\right)_o\right] + \left(Q_R\right)_M \tag{26}$$

$$\frac{\partial q_m}{\partial t} = - \left(\overline{\underset{\sim}{v}} \cdot \overline{\nabla q}_m\right)_M - \frac{1}{p_a - p_b}\left[\left(\overline{\omega' q'}\right)_a + k\frac{\Delta q}{\Delta s_v}\left(\overline{\omega' s_v'}\right)_o\right] \quad , \tag{27}$$

$$\frac{\partial p_b}{\partial t} = - \overline{\underset{\sim}{v}}_b \cdot \overline{\nabla p}_b + \overline{\omega}_b - \left(\overline{\omega}_\sigma\right)_b + \frac{k}{\Delta s_v}\left(\overline{\omega' s_v'}\right)_o \quad , \tag{28}$$

which are the equations which model the thermodynamics and thickness of the subcloud mixed layer.

2.2.2 Momentum Equations

We will assume that the clouds have no direct effect on the vertical eddy momentum flux in the mixed layer. In addition, we will assume that the Rossby number of the horizontally averaged flow is <<1, allowing us to write

$$\frac{\partial \bar{u}}{\partial t} = -\bar{\omega}\frac{\partial \bar{u}}{\partial p} + f\left(\bar{v} - \bar{v}_g\right) - \frac{\partial}{\partial p}\left(\overline{u'\omega'}\right) \quad , \tag{29a}$$

$$\frac{\partial \bar{v}}{\partial t} = -\bar{\omega}\frac{\partial \bar{v}}{\partial p} + f\left(\bar{u}_g - \bar{u}\right) - \frac{\partial}{\partial p}\left(\overline{v'\omega'}\right) \quad , \tag{29b}$$

which come from (3) and (4) with the horizontal advection of momentum neglected.

The observations of Lemone and Pennell (1974) imply that the vertical shear of the geostrophic wind in the lower atmosphere of the trade wind region can be too large to allow vertical uniformity of momentum in the subcloud mixed layer. Consequently, we will not assume that momentum is independent of pressure in the subcloud mixed layer. This prevents integration of (29) and (30) over mixed layer depth and requires computation of the pressure dependence of $\bar{u}$ and $\bar{v}$.

Thus, the pressure dependence of $\overline{\omega' u'}$ and $\overline{\omega' v'}$ must be parameterized in terms of mean field quantities. To accomplish this we adopt an eddy diffusion coefficient representation by assuming

$$\left.\begin{aligned} \overline{\omega' u'} &= -\rho^2 g^2 K^*(p) \frac{\partial \bar{u}}{\partial p} \\ \overline{\omega' v'} &= -\rho^2 g^2 K^*(p) \frac{\partial \bar{v}}{\partial p} \end{aligned}\right\} \quad \text{for} \quad p < p_1 \quad , \qquad (30)$$

where p_1 is the pressure at the first model gridpoint above the sea surface. Below level p_1 the eddy momentum flux is determined from the surface boundary layer theory discussed in Section 2.4.

We calculate the eddy diffusion coefficient, $K^*(p)$, from the model of O'Brien (1970). In this formulation the values of the diffusion coefficient and its derivative in the surface layer and at the top of the mixed layer are used to derive a Hermite-interpolating polynomial for $K^*(p)$ given by

$$K^*(p) = K^*(p_b) + \left(\frac{p_b - p}{p_b - p_1}\right)^2 \left\{ K^*(p_1) - K^*(p_b) + (p - p_a) \left[\frac{\partial}{\partial p} K^*(p)\Big|_{p_1} + 2\Big(K^*(p_1) - K^*(p_b)\Big)\Big/(p_b - p_1) \right] \right\} \quad , \qquad (31)$$

where $\frac{\partial K^*(p)}{\partial p}\Big|p_b$ is assumed zero and $K^*(p_b)$ is set to a small value characteristic of the free atmosphere. From surface boundary layer theory, $K^*(p_1)$ and $\frac{\partial K^*(p)}{\partial p}\Big|p_1$ are given by

$$K^*(p_1) = \frac{\kappa u_* \, z_1}{\phi_m\left(\frac{z_1}{L}\right)} \quad ,$$

$$\frac{\partial K^*(p)}{\partial p}\Big|_{p_1} = - \frac{\kappa u_*}{\rho_a \, g} \left[\frac{1}{\phi_m\left(\frac{z_1}{L}\right)} - \frac{z_1}{\phi_m^2\left(\frac{z_1}{L}\right)} \frac{\partial \phi_m\left(\frac{z_1}{L}\right)}{\partial z} \right] \quad . \quad (32)$$

The functional form of the nondimensional wind shear function, $\phi_m \frac{z}{L}$, is given in Section 2.4. This treatment of the eddy diffusion coefficient has been used by Pielke (1973) and Lee (1974).

2.3 THE CLOUD LAYER

2.3.1 Basic Equations

We now consider the heat and moisture conservation equations (1) and (2) applied in the cloud layer. We assume that $\overline{\omega's'}$, $\overline{\omega'q'}$, $\bar{c}$, and $\bar{e}$ above $p_{\bar{b}}$ are due solely to the presence of cumulus clouds that begin as updrafts originating from the mixed layer.

We neglect the accumulative storage of heat, water vapor, and liquid water in the cloud ensemble which implies that it is in a statistical steady state. This is an excellent assumption in the undisturbed trade wind regime and allows us to write the balance of liquid water between the environment and the cloud ensemble as

$$\bar{c} - \bar{e} - \frac{\partial}{\partial p}(\overline{\omega'\ell'})_\sigma - \overline{R^*} = 0 \quad , \tag{33}$$

where R* is the rate of raindrop generation per unit mass and the subscript σ indicates that the fluxes are due to clouds. Equation (33) can be used to transform (1) and (2) into

$$\frac{\partial \bar{s}}{\partial t} + \bar{\underline{v}}\cdot\nabla\bar{s} + \bar{\omega}\,\frac{\partial \bar{s}}{\partial p} = \bar{Q}_R + \frac{\partial}{\partial p}\left[L_v(\overline{\omega'\ell'})_\sigma - (\overline{\omega's'})_\sigma\right] + L_v\,\overline{R^*} \quad , \tag{34}$$

$$\frac{\partial \bar{q}}{\partial t} + \bar{\underline{v}}\cdot\nabla\bar{q} + \bar{\omega}\,\frac{\partial \bar{q}}{\partial p} = -\frac{\partial}{\partial p}\left[(\overline{\omega'q'})_\sigma + (\overline{\omega'\ell'})_\sigma\right] - \overline{R^*} \quad . \tag{35}$$

The quantities $(\overline{\omega' s'})_\sigma$, $(\overline{\omega' q'})_\sigma$, $(\overline{\omega' \ell'})_\sigma$, and $\overline{R^*}$ will be parameterized in terms of mean quantities as described in Section 2.3.2.

In the cloud layer, we again assume that the clouds do not produce a vertical flux of momentum and that the Rossby number is <<1. Hence, the equations for conservation of momentum in the cloud layer take the same form as (29)

2.3.2 Cumulus Parameterization

The cumulus parameterization theory used in this model is due to Arakawa and Schubert (1974). This theory provides a closed parameterization for the interaction of a cumulus cloud ensemble with the large-scale environment and will be reviewed here.

2.3.2.1 Spectral Representation of the Cumulus Ensemble

The cloud ensemble is spectrally divided into subensembles with all the clouds in a particular subensemble having the same constant fractional entrainment rate, λ, defined by

$$\lambda = \frac{-p}{\overline{H}\ \overline{\omega}_\sigma(\lambda,p)} \frac{\partial \overline{\omega}_\sigma}{\partial p}(\lambda,p) \quad , \qquad (36)$$

where $\overline{\omega}_\sigma(\lambda,p)$ is the average vertical p-velocity inside the clouds in subensemble λ at level p multiplied times the

fractional part of the model domain covered by subensemble , and $\bar{H} \equiv R\bar{T}/g$. It is convenient to express $\bar{\omega}_\sigma(\lambda,p)$ as

$$\bar{\omega}_\sigma(\lambda,p) = - g\, n(\lambda,p)\, m_b(\lambda)\, d\lambda \quad , \tag{37}$$

where $m_b(\lambda)\, d\lambda$ is the summation of the instantaneous cloud-induced vertical mass fluxes at p_b over all the clouds in subensemble λ and $n(\lambda,p)$ is a nondimensional normalizing function, equal to 1 at p_b. Equations (36) and (37) can be combined to yield

$$\frac{\partial n}{\partial p}(\lambda,p) = - \frac{\lambda \bar{H}}{p}\, n(\lambda,p) \quad , \tag{38}$$

which is a differential equation expressing conservation of mass for the subensemble that can be solved for $n(\lambda,p)$.

Cloud tops are taken to be the level of vanishing buoyancy, $p_d(\lambda)$, and the subensemble is assumed to have a thin layer of detrainment at this level in which the vertical mass flux goes to zero. Thus, $n(\lambda,p) \equiv 0$ for $p \leq p_d(\lambda)$.

Note that since the members of the subensemble are assumed to be at random phases in their life cycle, $m_b(\lambda)\, d\lambda$ is proportional to the mass flux of a single cloud in subensemble λ averaged over its entire lifetime, with the constant of proportionality equal to the number of clouds in the subensemble. Note also that because of the effect of entrainment on cloud buoyancy and from the entrainment-radius relationship (see Simpson, 1971), small λ corresponds to deep clouds with large radii and large λ corresponds to shallow clouds with small radii (see Figure 1).

Now, again invoking the assumption that the fractional area covered by active clouds is small, the total cloud-induced vertical fluxes of mass, dry static energy, water vapor, and liquid water averaged horizontally across the model domain can be written (Schubert, 1974)

$$\bar{\omega}_\sigma(p) = - g \int_o^{\lambda_d(p)} n(\lambda,p)\, m_b(\lambda)\, d\lambda \quad , \tag{39}$$

$$(\overline{\omega' s'})_\sigma = - g \int_o^{\lambda_d(p)} n(\lambda,p) \left| s_\sigma(\lambda,p) - \bar{s}(p) \right| m_b(\lambda)\, d\lambda \quad , \tag{40}$$

$$(\overline{\omega' q'})_\sigma = - g \int_o^{\lambda_d(p)} n(\lambda,p) \left| q_\sigma(\lambda,p) - \bar{q}(p) \right| m_b(\lambda)\, d\lambda \quad , \tag{41}$$

$$(\overline{\omega' \ell'})_\sigma = - g \int_o^{\lambda_d(p)} n(\lambda,p)\, l(\lambda,p)\, m_b(\lambda)\, d\lambda \quad , \tag{42}$$

where $s_\sigma(\lambda,p)$, $q_\sigma(\lambda,p)$, and $\ell(\lambda,p)$ are the dry static energy, water vapor mixing ratio, and liquid water mixing ratio inside type λ clouds at level p and $\lambda_d(p)$ is the entrainment rate of the clouds whose tops are at level p. Thus, the total cloud-induced flux of a particular quantity at level p is an integral of the subensemble fluxes of this quantity over all the subensembles which penetrate level p.

In addition, we can express the ensemble average raindrop generation rate by

$$\overline{R}^{*}_{\sigma} = \int_{0}^{\lambda_d(p)} n(\lambda,p)\, r(\lambda,p)\, m_b(\lambda)\, d\lambda \quad , \qquad (43)$$

where $r(\lambda,p)$ is the raindrop generation rate for subensemble λ at level p per unit cloud mass flux. We will parameterize $r(\lambda,p)$ by

$$r(\lambda,p) = C_o\, \ell(\lambda,p) \quad , \qquad (44)$$

where C_o is a constant. Furthermore, we neglect the re-evaporation of raindrops and assume that all the detrained liquid water evaporates into the environment immediately.

To close the cumulus parameterization theory, $s_\sigma(\lambda,p)$, $q_\sigma(\lambda,p)$, $\ell(\lambda,p)$, and $m_b(\lambda)$ must be determined as a function of the large-scale quantities. This can be achieved from the considerations which follow.

2.3.2.2 Prediction of the Thermodynamic Properties of the Clouds

The equations for conservation of heat, water vapor, and liquid water in subensemble λ can be written (Schubert, 1974)

$$\frac{\partial}{\partial p}\left[n(\lambda,p)\, s_\sigma(\lambda,p)\right] + \frac{\overline{H}\, n(\lambda,p)}{p}\left[\lambda s(p) + L_v\, c(\lambda,p)\right] = 0 \qquad (45)$$

$$\frac{\partial}{\partial p}\left[n(\lambda,p)\, q_\sigma(\lambda,p)\right] + \frac{\bar{H}\, n(\lambda,p)}{p}\left[\lambda\bar{q}(p) - c(\lambda,p)\right] = 0 \tag{46}$$

$$\frac{\partial}{\partial p}\left[n(\lambda,p)\, \ell(\lambda,p)\right] + \frac{\bar{H}\, n(\lambda,p)}{p}\left[c(\lambda,p) - r(\lambda,p)\right] = 0 \tag{47}$$

The first terms on the left-hand sides of (45) through (47) represent convergence of heat, moisture, and liquid water, respectively, in the subensemble per unit cloud mass flux. The terms in (45) and (46) which have λ as a factor represent entrainment of environmental heat and moisture, respectively, per unit cloud mass flux. Finally, the second and third terms in (47) represent the liquid water source due to condensation and the liquid water sink due to raindrop formation in the subensemble per unit cloud mass flux. Note that radiational heating inside the clouds has been neglected, which is reasonable since it is small compared to the other terms in (45). Equations (45) through (47) are valid in the region $p_b \geq p > p_d(\lambda)$.

Equations (45) and (46) can be combined to yield

$$\frac{\partial}{\partial p}\left[n(\lambda,p)\, h_\sigma(\lambda,p)\right] + \frac{\lambda n(\lambda,p)}{p}\,\bar{H}\,\bar{h}(p) = 0 \quad , \tag{48}$$

where $h_\sigma(\lambda,p)$ is the moist static energy of the clouds given by

$$h_\sigma(\lambda,p) = s(\lambda,p) + L_v\, q_\sigma(\lambda,p) \quad , \tag{49}$$

and $\bar{h}(p)$ is the moist static energy of the environment given by

$$\bar{h}(p) = \bar{s}(p) + L_v \bar{q}(p) \quad , \tag{50}$$

Similarly, (46) and (47) can be combined to yield

$$\frac{\partial}{\partial p}\left\{n(\lambda,p)\left[q_\sigma(\lambda,p) + \ell(\lambda,p)\right]\right\} +$$

$$\frac{\lambda n(\lambda,p)}{p} \bar{H}\, \bar{q}(p) - \frac{\bar{H}\, n(\lambda,p)}{p} r(\lambda,p) = 0 \quad . \tag{51}$$

Furthermore, above cloud base $q_\sigma(\lambda,p)$ can be determined from the saturation condition

$$q_\sigma(\lambda,p) = \bar{q}^*(p) + \frac{\gamma}{1+\gamma}\frac{1}{L_v}\left[h_\sigma(\lambda,p) - \overline{h^*}(p)\right], \tag{52}$$

where $\bar{q}^*(p)$ is the saturation mixing ratio of the environment, $h^*(p)$ is the saturated moist static energy of the environment

$$\overline{h^*}(p) = \bar{s}(p) + L_v \overline{q^*}(p) \quad , \tag{53}$$

and

$$\gamma \equiv \frac{L_v}{c_p}\left(\frac{\partial q^*}{\partial T}\right)_p \quad . \tag{54}*$$

*(See Arakawa and Schubert, 1974)

The analytical forms for q* and λ used in this model are given in Appendix B.

From our assumption that the clouds have "roots" extending down into the mixed layer which is consistent with the observations of Pennel and Lemone (1976), we take

$$s_\sigma(\lambda,p_b) = s_m \quad , \tag{55}$$

$$q_\sigma(\lambda,p_b) = q_m \quad . \tag{56}$$

We further assume p_c to be at the lifting condensation level and note that

$$\ell(\lambda,p) = 0 \qquad \text{for } p \geq p_c \quad . \tag{57}$$

Equation (44) along with the differential equations (48) and (51) and the boundary conditions (55) through (57), allow prediction of the thermodynamic properties of the cloud ensemble in the following manner. For $p_c < p < p_b$, (48) and (51) are integrated upwards from p_b taking into account (55) through (57). From the values of $h_\sigma(\lambda,p)$ and $q_\sigma(\lambda,p)$ so obtained, $s_\sigma(\lambda,p)$ can be determined from (49). For $p_c > p > p_d(\lambda)$, (48) and (51) are integrated upwards from p_c with consideration of (44). This, along with (52) and (38) yields $s_\sigma(\lambda,p)$, $q_\sigma(\lambda,p)$, and $\ell(\lambda,p)$. Cloud tops are assumed to occur where the clouds lose buoyancy which implies

$$s_{v\sigma}\left(\lambda_d(p),p\right) = \bar{s}_v(p) \quad , \tag{58}$$

at $p = p_d(\lambda)$, where $\bar{s}_v(p)$ is given by (21) and

$$s_{v\sigma}(\lambda,p) - s_\sigma(\lambda,p) + c_p \bar{T}\left(0.61q\ (\lambda,p) - \ell(\lambda,p)\right) \quad . \tag{59}$$

2.3.2.3 Prediction of $m_b(\lambda)$

The cumulus parameterization will be closed if we can predict the cloud-induced vertical mass flux at p_b, $m_b(\lambda)$. To do this we introduce the "cloud work function", $A(\lambda)$, given by

$$A(\lambda) = -\frac{R}{c_p} \int_{p_b}^{p_d(\lambda)} n(\lambda,p) \left(s_{v\sigma}(\lambda,p) - s_v(p)\right) \frac{dp}{p} \ , \tag{60}$$

which is simply an integral measure of the buoyancy force for cloud type λ weighted with the function $n(\lambda,p)$. The time derivative of $A(\lambda)$ can be written in the form

$$\frac{dA(\lambda)}{dt} = \int_0^{\lambda_{max}} K(\lambda,\lambda')\ m_b(\lambda')\ d\lambda' + F(\lambda) \quad , \tag{61}$$

where $K(\lambda,\lambda')$ and $F(\lambda)$ can both be expressed in terms of large-scale quantities alone.

The term $F(\lambda)$ in (61) is the rate at which the large-scale forcing increases the cloud work function for subensemble . The dominant effects in $F(\lambda)$ are typically

cooling above cloud base due to infrared radiation and adiabatic expansion. The kernel, $K(\lambda,\lambda')$ is the rate at which type λ' clouds increase the cloud work function for type λ clouds per unit cloud mass flux. It is generally negative and the dominant effect it represents is warming above cloud base due to adiabatic compression associated with compensating subsidence in the environment between the clouds. Hence, the first term on the right-hand side of (61) represents the rate at which the cumulus ensemble decreases the cloud work function for subensemble λ through release of the moist convective instability.

Arakawa and Schubert (1974) demonstrate that in the tropics the time scale for changes in the large-scale forcing is much longer than the time scale for the cloud ensemble to adjust to the forcing. This implies that the cumulus ensemble follows a sequence of quasi-equilibria with the large-scale forcing. Furthermore, the cloud work function in this set of quasi-equilibria remains approximately constant in time at some relatively small value. Thus, (61) can be written

$$\int_0^{\lambda_{max}} K(\lambda,\lambda')\, m_b(\lambda')\, d\lambda' + F(\lambda) \cong 0 \quad . \qquad (62)$$

The kernel, $K(\lambda,\lambda')$ can be expressed as the sum of three parts

$$K(\lambda,\lambda') = K_V(\lambda,\lambda') + K_D(\lambda,\lambda') + K_M(\lambda) \quad . \qquad (63)$$

The "vertical mass flux kernel", $K_V(\lambda,\lambda')$, accounts for the decrease of the cloud work function for type λ clouds due to compensating subsidence in the environment and is the dominant effect in $K(\lambda,\lambda')$ as mentioned earlier. The "detrainment kernel", $K_D(\lambda,\lambda')$, accounts for the increase of the cloud work function for type λ clouds due to cooling and moistening of the environment caused by detrainment of liquid water and saturated air from shallower clouds. The "mixed layer kernel", $K_M(\lambda)$ accounts for the decrease of the cloud work function for type λ clouds due to changes in the thermodynamic characteristics and thickness of the mixed layer.

Analytical expressions for $K_V(\lambda,\lambda')$, $K_D(\lambda,\lambda')$, $K_M(\lambda)$, and $F(\lambda)$ can be obtained by formally taking the time derivative of (60) and making use of earlier expressions. The details of this calculation are given in Arakawa and Schubert (1974) and, because of their great complexity, will not be presented here.

For use of the theory in a numerical prediction model, it is unnecessary to evaluate an analytical expression for $F(\lambda)$. Rather, it is convenient to replace $F(\lambda)$ by the equivalent expression

$$F(\lambda) = \frac{A_{LS}(\lambda)}{\Delta t} \quad ,$$

where $A_{LS}(\lambda)$ is the cloud work function produced by the large-scale forcing alone during one time step, Δt, of the model. Hence, (62) can be written

$$G(\lambda) = \int_{o}^{\lambda_{max}} K(\lambda,\lambda') \, m_b(\lambda) \, d\lambda' + \frac{A_{LS}(\lambda)}{\Delta t} = 0 \quad . \tag{64}$$

Using (60), (63), and the expressions in Appendix B of Arakawa and Schubert (1974), equation (64) (which is a Fredholm integral equation of the first kind) is solved for $m_b(\lambda)$, subject to the constraints

$$m_b(\lambda) = 0 \quad \text{for} \quad A(\lambda) \leq 0 \quad \text{or} \quad G(\lambda) < 0$$

$$m_b(\lambda) > 0 \quad \text{for} \quad G(\lambda) \geq 0 \quad . \tag{65}$$

Additional changes in $\bar{s}$ and $\bar{q}$ are then calculated from the cloud terms in (36) and (37). The integral equation, (64), is solved with a simple iterative scheme described in Appendix C which is similar to that discussed by Schubert (1973).

Note that this cumulus parameterization theory does not explicitly predict σ. Following Ogura and Cho (1973), however, we can estimate σ by assuming that the magnitude of the vertical velocity of the updrafts entering the clouds at p_b, w_b, is independent of λ and σ. Thus we have

$$\sigma = - \frac{\left(\bar{\omega}_\sigma\right)_b}{p_b \; g \; w_b} \quad . \tag{66}$$

As an estimate of the fractional cloud coverage, where p_b is the density of the air at p_b and $(\omega_\sigma)_b$ is calculated from (39). Ogura and Cho found w_b to be about 1 m s^{-1} from their diagnostic calculations, which is the value used in this model.

2.3.2.4 Detrainment Form of the Cumulus Parameterization Theory

It is instructive to write the cloud terms of (34) and (35) in "detrainment form" (see Schubert, 1974). Differentiating (40) through (42) with respect to p and making use of (38) and (45) through (47), the conservation equations for heat and moisture, (34) and (35), can be written

$$\frac{\partial \bar{s}}{\partial t} + \bar{\underline{v}}\cdot\overline{\nabla s} + \bar{\omega}\frac{\partial \bar{s}}{\partial p} = \bar{Q}_R + D(p)\left|\hat{s} - \bar{s} - L\hat{\ell}\right| + \bar{\omega}_\sigma(p)\,\frac{\partial \bar{s}}{\partial p} \quad , \tag{67}$$

$$\frac{\partial \bar{q}}{\partial t} + \bar{\underline{v}}\cdot\overline{\nabla q} + \bar{\omega}\frac{\partial \bar{q}}{\partial p} = D(p)\left|\hat{q} - \bar{q} + \hat{\ell}\right| + \bar{\omega}_\sigma(p)\,\frac{\partial \bar{q}}{\partial p} \quad , \tag{68}$$

where the D(p) is total detrainment rate for the ensemble given by

$$D(p) = g\, m_b\left(\lambda_d(p)\right)\, n\left(\lambda_d(p), p\right)\, \frac{d\lambda_d(p)}{dp} \quad . \tag{69}$$

and

$$\hat{s}(p) = s_\sigma\left(\lambda_d(p),p\right) \quad ,$$

$$\hat{q}(p) = q_\sigma\left(\lambda_d(p),p\right) \quad ,$$

$$\hat{\ell}(p) = \ell\left(\lambda_d(p),p\right) \quad . \tag{70}$$

The total detrainment rate is zero below the lowest detrainment level. Thus, below this level the ensemble modifies the large-scale fields simply through cloud-induced subsidence in the environment as represented by the terms $\bar{\omega}_\sigma(p)\,\frac{\partial \bar{s}}{\partial p}$ and $\bar{\omega}_\sigma(p)\,\frac{\partial \bar{q}}{\partial p}$ in (67) and (68).

2.4 THE SURFACE LAYER

Under steady, convectively unstable, horizontally homogeneous conditions, Monin-Obukhov similarity theory predicts that a surface layer of thickness -L exists in which the eddy fluxes depart little from their surface values and properly scaled derivatives of temperature, moisture and momentum are universal functions of z/L. Here, z is the height above the surface and L is the Monin-Obukhov length defined by (see Kraus, 1972)

$$L = \frac{\rho_a \, u_*^3}{\kappa\left[\frac{(\overline{\omega' s'})_o}{c_p \, T_o} + 0.61(\overline{\omega' q'})_o\right]} \quad , \tag{71}$$

where u_* is the surface friction velocity given by

$$u_* = \left(\frac{|\vec{\tau}_o|}{\rho_a}\right)^{\frac{1}{2}} \quad , \tag{72}$$

and $_o$ is the surface wind stress vector. Other symbols are defined in Appendix A. Note that L is negative in a convectively unstable boundary layer which is the case we restrict our attention to here.

Thus, in the surface layer we have

$$\frac{\partial \overline{\theta}}{\partial z} = \frac{(\overline{\omega' s'})_o \, \phi_\theta\left(\frac{z}{L}\right)}{\rho_a \, g \, \kappa u_* \, z \, c_p} \quad , \tag{73}$$

$$\frac{\partial \bar{q}}{\partial z} = \frac{(\overline{\omega' q'})_o \, \phi_q\left(\frac{z}{L}\right)}{\rho_a \, g \, \kappa u_* \, z} \quad , \tag{74}$$

$$\frac{\partial \bar{U}}{\partial z} = \frac{u_*}{\kappa z} \, \phi_m\left(\frac{z}{L}\right) \quad , \tag{75}$$

where $\bar{U}$ is wind speed. The forms of the ϕ functions have been reviewed by Högstrom (1974) and it is generally accepted that most atmospheric data are well represented by

$$\left.\begin{aligned} \phi_\theta = \phi_q &= \left(1 - 9\,\frac{z}{L}\right)^{-\frac{1}{2}} \\ \phi_m &= \left(1 - 15\,\frac{z}{L}\right)^{-\frac{1}{4}} \end{aligned}\right\} \quad \text{for} \quad L < 0 \quad , \tag{76}$$

which are the forms used here.

Using (76), the profile relations (73) through (75) can be integrated from z_o, the surface roughness length, to z (see Paulson, 1970)

$$\bar{\theta}(z) = \theta_o + \frac{(\overline{\omega' s'})_o}{\rho_a \, g \, \kappa u_* \, c_p} \left[\ln\left(\frac{z}{z_o}\right) - 2 \ln\left(\frac{1 + y_\theta^2}{2}\right)\right] \quad , \tag{77}$$

$$\bar{q}(z) = q_o + \frac{(\overline{\omega' q'})_o}{\rho_a \, g \, \kappa u_*} \left[\ln\left(\frac{z}{z_o}\right) - 2 \ln\left(\frac{1 + y_q^2}{2}\right) \right] , \qquad (78)$$

$$\bar{U}(z) = U_o + \frac{u_*}{\kappa} \left[\ln\left(\frac{z}{z_o}\right) - 2 \ln\left(\frac{1 + y_m}{2}\right) - \ln\left(\frac{1 + y_m^2}{2}\right) + 2 \tan^{-1} y_m - \tfrac{1}{2}\pi \right] , \qquad (79)$$

where θ_o, q_o, and U_o are potential temperature, water vapor mixing ratio, and wind speed at z_o, and

$$y_\theta = y_q = \left(1 - 9 \frac{z}{L}\right)^{\frac{1}{4}} , \qquad (80)$$

$$y_m = \left(1 - 15 \frac{z}{L}\right)^{\frac{1}{4}} . \qquad (81)$$

At a height of -L, $\bar{\theta}$ and $\bar{q}$ are given, to excellent approximation, by their mixed layer values. Thus, setting z = -L in (77) and (78) yields, after rearrangement

$$(\overline{\omega' s'})_o = \kappa u_* \, c_p \, \rho_a \, g \, \frac{(\theta_m - \theta_o)}{\left[\ln\left(\frac{-L}{z_o}\right) - 1.466\right]} = g \, H_o , \qquad (82)$$

and

$$(\overline{\omega' q'})_o = \kappa u_* \rho_a g \frac{(q_m - q_o)}{\left[\ln\left(\frac{-L}{z_o}\right) - 1.466\right]}$$

$$= g Q_o \quad , \tag{83}$$

where H_o is the surface sensible heat flux and $L_v Q_o$ is the surface latent heat flux (both taken positive downward). Since we do not assume that momentum is uniform in the mixed layer it is not advantageous to integrate (75) to the top of the surface layer. Rather, we integrate (75) from z_o to z_1 where z_1 is the height of the first model gridpoint and $z_1 < -L$. Thus, (79) yields after rearrangement

$$u_* = \kappa (U_1 - U_o) \Big/ \left[\ln \frac{z_1}{z_o} - 2 \ln\left(\frac{1 + y_1}{2}\right) - \ln\left(\frac{1 + y_1^2}{2}\right) + 2 \tan^{-1} y_1 - \tfrac{1}{2}\pi\right] \quad , \tag{84}$$

where U_1 is the wind speed at the first model gridpoint, U_o is the wind speed at z_o, and

$$y_1 = \left(1 - \frac{9 z_1}{L}\right)^{\frac{1}{4}} \quad . \tag{85}$$

Following Clarke (1970) and others, we assume that the roughness length for the sea surface is given by

$$z_o = \max\left(0.032\ u_*^2/g,\ z_{min}\right) \quad , \tag{86}$$

where $z_{min} = 0.0015$ cm. We set θ_o equal to the sea surface temperature and q_o equal to 0.98 times the saturation value at the sea surface to account for the effect of salinity on the vapor pressure of water (see Roll, 1971). We set U_o equal to the surface drift velocity which is approximated by (Kraus,1977)

$$\underset{\sim}{v}_o = \left(\frac{\rho_a}{\rho_w}\right)^{\frac{1}{2}} \underset{\sim}{v}_{og} + \underset{\sim}{v}_c \quad , \tag{87}$$

where ρ_a and ρ_w are reference densities for air and water, $\underset{\sim}{v}_{og}$ is the mean current vector in the upper layer of the ocean. The direction of the surface wind stress vector is assumed to be that of the wind at z_1. The wind vector at z_1 is predicted by (29) and (30). Thus, using the fact that

$$\theta_m = \frac{s_m}{c_p} \quad , \tag{88}$$

which follows from (6), (12), and (13), equations (82) through (88) allow prediction of the surface fluxes of heat, moisture, and momentum in terms of model-predicted quantities. We solve (71), (72) and (82) through (86) iteratively at each time step and assume

$$\left.\begin{aligned} (\overline{\omega' s'}) &= (\overline{\omega' s'})_o \\ (\overline{\omega' q'}) &= (\overline{\omega' q'})_o \end{aligned}\right\} \quad \text{for} \quad p \geq p_a \ , \tag{89}$$

$$\left.\begin{aligned} (\overline{\omega' u'}) &= - g \tau_o^x \\ (\overline{\omega' v'}) &= - g \tau_o^y \end{aligned}\right\} \quad \text{for} \quad p \_ p_a \ , \tag{90}$$

where p_a is the pressure at the top of the surface layer.

2.5 RADIATIVE TRANSFER EQUATIONS

The net radiational heating rate of the atmosphere averaged across the model domain can be written

$$\bar{Q}_R = - g \left[(1 - \sigma) \frac{\partial}{\partial p} \left(F^*_{CLR} + S^*_{CLR} \right) + \sigma \frac{\partial}{\partial p} \left(F^*_{CLD} + S^*_{CLD} \right) \right] , \quad (91)$$

where F^*_{CLR} and S^*_{CLR} are the net downward fluxes of long- and short-wave radiation in the clear region, and F^*_{CLD} and S^*_{CLD} are the net downward fluxes in the cloudy region. Note that since $\sigma << 1$ for the physical system to be modeled, the net radiational heating due to the presence of clouds is very small. Thus, (91) can be written to excellent approximation as

$$\bar{Q}_R = - g \frac{\partial}{\partial p} \left(F^*_{CLR} + S^*_{CLR} \right) . \quad (92)$$

We calculate the long- and short-wave fluxes in the manner described in the next two sections.

2.5.1 Long-Wave Radiative Flux

Using the approximations of Danard (1969), we calculate the terrestrial long-wave radiative flux at level p in the clear region from

$$F^*(p)_{CLR} = - \varepsilon_o B \bar{T}_o^4 +$$

$$\frac{B}{g}\left[\int_{p_e}^{p} \bar{T}^4(p')\,\varepsilon^*(p,p')\,\bar{q}(p')\left(\frac{p'}{p_r}\right)^{0.85}\left(\frac{T_r}{\bar{T}(p')}\right)^{0.5} dp'\right.$$

$$\left. + \int_{p}^{p_o}\left(\varepsilon_o \bar{T}_o^4 - \bar{T}^4(p')\right)\varepsilon^*(p,p')\,\bar{q}(p')\left(\frac{p'}{p_r}\right)^{0.85}\left(\frac{T_r}{\bar{T}(p')}\right)^{0.5} dp'\right]$$

$$\text{for} \quad p_e \leq p \leq p_o \quad , \tag{93}$$

where B is the Stefan-Boltzmann constant, ε_o is the emissivity of the sea surface, T_r is a reference temperature, p_r is a *reference pressure*, p_e is the pressure at the top of the model, and

$$\varepsilon^*(p,p') = \varepsilon'(|w(p) - w(p')|) \quad .$$

Here, w(p) is the pressure corrected precipitable water vapor defined by

$$w(p) = \frac{1}{g}\int_{o}^{p} \bar{q}(p')\left(\frac{p'}{p_r}\right)^{0.85}\left(\frac{T_r}{\bar{T}(p')}\right) dp' \quad , \tag{94}$$

and

$$\varepsilon' = \frac{d\varepsilon}{dw}(w) \quad . \tag{95}$$

We assume that the precipitable water at p_e is a constant and we approximate ε' by fitting Elsasser's (1960) experimental curve for the flux emissivity of pure water vapor, ε, with an analytical function.

The first term on the right-hand side of (93) is the black body emission from the sea surface. The first and second integrals on the right-hand side of (93) represent the contribution to the long-wave flux at level p due to emission and absorption of radiation above and below level p respectively. See Haltiner (1971) for a detailed discussion of this radiative transfer model.

Note that, although (92) and (93) give a good prediction of $\bar{Q}_R$, this long-wave radiative transfer model overestimates the infrared cooling of the sea surface. Consequently we use the empirical relationship of Reed (1976) to calculate the net long-wave flux at the sea surface. Thus

$$F_o^* = {}_o\, \bar{T}_o^4\, 0.254 - 0.811\, q_{10} \quad , \tag{96}$$

where q_{10} is the water vapor mixing ratio at 10 m height and is calculated from the profile relation (78).

2.5.2 Short-Wave Radiative Flux

Following Arakawa, Katayama, and Mintz (1968), we assume the short-wave radiation to consist of two parts: (a) with wavelength less than 0.9 μ in which Rayleigh scattering is significant but absorption by water vapor is

negligible, and (b) with wavelength greater than 0.9 μ in which absorption by water vapor is significant but scattering is slight. In this formulation the incident radiation is partitioned according to

$$S_o^S = 0.651\ S_o \cos\alpha$$

$$S_o^A = 0.349\ S_o \cos\alpha \quad , \tag{97}$$

where S_o is the net incident solar radiation at the model top, $S_o^{S_o}$ is the downward flux of solar radiation subject to scattering, S_o^A is the downward flux of solar radiation subject to absorption, and α is the Zenith angle. Then, $S^*_{CLR}(p)$ is represented by the empirical relationship

$$S^*_{CLR}(p) = S_o^A \left[1 - C_s\left(w^*(p)\ \sec\alpha\right)^{0.303}\right] + S_o^S \left[\frac{1 - a_o}{1 - a_o a_s}\right]$$

$$\text{for} \quad p_e \le p \le p_o \quad , \tag{98}$$

where a_o is the albedo of the scattered radiation and is taken to be

$$a_o = 0.085 - 0.245 \log\left(\frac{p_o}{p_e}\cos\alpha\right) \quad , \tag{99}$$

and

$$w^*(p) = w\left(p_o\right) - w(p) \quad . \tag{100}$$

C_s is a constant, and a_s is the albedo of the sea surface. The expression $(1 - a_o a_s)$ in the denominator of the second term on the right-hand side of (98) is present to model the enhancement of the downward flux of radiation due to back scattering from multiple reflections. This short-wave radiative transfer model is described in more detail by Haltiner (1971).

In order to determine the daily-averaged value of the solar heating rather than the instantaneous value, $S_o \cos \alpha$ is averaged over 24 hours with the constraint $S_o \cos \alpha = 0$ for $\alpha > \frac{1}{2}\pi$ and $\alpha < -\frac{1}{2}\pi$. This yields

$$\langle S_o \cos \alpha \rangle = S_o \left[\frac{(\sin \phi \sin \delta)\, \Omega}{\pi} + \frac{(\cos \phi \cos \delta)}{2\pi} \int_{-\Omega}^{\Omega} \cos \xi \, d\xi \right] , \qquad (101)$$

where

ϕ = latitude at center of model domain

δ = declination angle of sun

$\Omega = \cos^{-1} \left(\tan \phi \tan \delta \right)$,

and $\langle\ \rangle$ indicates the average over 24 hours. We use $\langle S_o \cos \alpha \rangle$ in (97) through (99) and, although this is not exactly equivalent to averaging (97) through (99) over 24 hours, it is adequate for our purposes.

Finally, the net short-wave flux at the sea surface is calculated from

$$S_o^* = S_{CLR}^*(p_o) \quad , \tag{102}$$

where again we have made use of the fact that $\sigma << 1$ for the cases to be considered here.

2.6 ONE-DIMENSIONAL REPRESENTATION

We will adopt a one-dimensional model by integrating equations (26) through (30) and (34) and (35) with $\overline{\underline{v}}\cdot\overline{\nabla q}$, $\overline{\underline{v}}_b\cdot\overline{\nabla p}_b$, $\overline{u}_g$, $\overline{v}_g$, $\overline{\omega}$, p_o, and the sea surface temperature imposed. Note that specification of the vertical profile of the geostrophic wind implies $\overline{\nabla s}$ in the following manner.

$$f\overline{u}_g = -\,g\left(\frac{\partial z}{\partial y}\right)_p \quad , \tag{103}$$

$$f\overline{v}_g = g\left(\frac{\partial z}{\partial x}\right)_p \quad , \tag{104}$$

and the horizontally averaged thermal wind equations with the effect of moisture on density neglected

$$\frac{\partial \overline{u}_g}{\partial p} = \frac{R}{fp}\left(\frac{\partial \overline{T}}{\partial y}\right)_p \quad , \tag{105}$$

$$\frac{\partial \overline{v}_g}{\partial p} = -\,\frac{R}{fp}\left(\frac{\partial \overline{T}}{\partial x}\right)_p \quad , \tag{106}$$

the horizontally averaged gradient of dry static energy on a level of constant pressure can be written

$$\overline{\nabla s} = \left(- \frac{c_p fp}{R} \frac{\partial \bar{v}_g}{\partial p} + f\bar{v}_g \right) \hat{i}$$

$$+ \left(\frac{c_p fp}{R} \frac{\partial \bar{u}_g}{\partial p} - f\bar{u}_g \right) \hat{j} \quad , \qquad (107)$$

where $\hat{i}$ and $\hat{j}$ are unit vectors in the x and y directions. Hence, the horizontally averaged horizontal advection of dry static energy can be written

$$\underset{\rightarrow}{\bar{v}} \cdot \overline{\nabla s} = \bar{u} \left(- \frac{c_p fp}{R} \frac{\partial \bar{v}_g}{\partial p} + f\bar{v}_g \right)$$

$$+ \bar{v} \left(\frac{c_p fp}{R} \frac{\partial \bar{u}_g}{\partial p} - f\bar{u}_g \right) \quad . \qquad (108)$$

Thus, the horizontal advection of heat is included in a self-consistent fashion.

For all of the experiments reported here we will set $\underset{\rightarrow}{\bar{v}} \cdot \overline{\nabla q}$ equal to zero. This is a fairly good assumption for the undisturbed trade wind regime. For example, Esbensen (1975) analyzed the BOMEX data and found that the eddy flux of moisture at the top of the mixed layer nearly balanced the sea surface evaporation during the period of his study. This along with the well-known steadiness of the trade wind thermodynamic structure, implies that the horizontal advection of moisture in the mixed layer is, on the average, relatively small compared to the other processes that contribute to the mixed layer moisture balance.

In addition, we set $\overline{\underline{v}}_b \cdot \overline{\nabla p}_b$ equal to zero in all of the experiments reported here. This is a good assumption since the mixed layer thickness tends to be spatially uniform in the undisturbed trade wind regime. Consequently, the contribution of $\overline{\underline{v}}_b \cdot \overline{\nabla p}_b$ in (28) is expected to be negligible compared to the other terms.

2.7 COMPUTATIONAL CONSIDERATIONS

2.7.1 Model Grid

In order to resolve the surface layer without demanding unnecessary core storage, a vertically stretched grid is employed with the stretching function given by

$$p_j = p_o\left[1 - b_1 j^2 - b_2 j\right] \quad , \qquad (109)$$

with

$$b_1 = 1.106 \times 10^{-3} \quad ,$$

and

$$b_2 = 1.175 \times 10^{-3} \quad .$$

Values of s, q, u, and v are computed at levels defined by setting j = 1,2,3,...,28 in (109). This choice of parameters places the first gridpoint at approximately 20 m above the sea surface and the last gridpoint at about tropopaule level. The upper boundary conditions on the prognostic variables are given in Table 1.

Note that p_b as determined by (28) does not fall at a model gridpoint in general. Hence, in order to calculate Δs and Δq, we utilize a "floating gridpoint" at $p_{\overline{b}}$ which moves up and down with the top of the mixed layer. Assuming no clouds detrain at $p_{\overline{b}}$, we can write

TABLE 1. Model Constants for All Three Sets of Experiments

CONSTANT	SYMBOL	VALUE
E-W component of wind at model top	u_e	3 m s^{-1}
N-S component of wind at model top	v_e	v_g
Water vapor mixing ratio at model top	q_e	0.05 g kg^{-1}
Temperature at model top	T_e	206 K
Emissivity at sea surface	ε_o	0.97
Short-wave flux at model top	S_o	2.21×10^3 cal cm^{-2} day^{-1}
Empirical constant for absorption of solar radiation	C_s	0.02
Albedo of sea surface	a_s	0.065

TABLE 1. (Continued)

CONSTANT	SYMBOL	VALUE
Latitude	Φ	15^{o}
Declination angle of sun	δ	20^{o}
Fractional entrainment rate for subensembles	λ_j, $j = 1,2,\ldots,5$	0,5,10,15,20% km^{-1}
Vertical velocity of updrafts entering the clouds at p_b	w_b	1 m s^{-1}
Reference density for air	ρ_a	1.18 kg m^{-3}
Reference density for water	ρ_w	10^3 kg m^{-3}
Raindrop generation rate parameter	C_o	5×10^{-4} m^2 kg^{-1}

TABLE 1. (Continued)

CONSTANT	SYMBOL	VALUE
Eddy diffusion coefficient for momentum at and above p_b	$K^*(p_b)$	$1\ m^2\ s^{-1}$
Mean current vector in upper layer of the ocean	$\underline{v}_c$	0
Reference temperature for atmosphere	T_r	273 K
Entrainment parameter	k	0.1
Reference pressure	p_r	1010 mb
Surface pressure	p_o	1010 mb
Pressure at model top	p_e	100 mb
von Karman's constant	κ	0.4

$$\frac{\partial \bar{s}\left(p_{\bar{b}}\right)}{\partial t} = -\left(\bar{\underline{v}}_b \cdot \nabla \bar{s}_b\right)$$

$$+ \frac{\partial \bar{s}\left(p_b\right)}{\partial p}\left[\left(\bar{\omega}_\sigma\right)_b - \bar{\omega}_b + \frac{\partial p_b}{\partial t}\right]$$

$$+ \bar{Q}_R\left(p_{\bar{b}}\right) \qquad (110)$$

$$\frac{\partial \bar{q}\left(p_{\bar{b}}\right)}{\partial t} = -\left(\bar{\underline{v}}_b \cdot \nabla q_b\right)$$

$$+ \frac{\partial \bar{q}\left(p_b\right)}{\partial p}\left[\left(\bar{\omega}_\sigma\right)_b - \bar{\omega}_b + \frac{\partial p_b}{\partial t}\right] \quad . \qquad (111)$$

With $\bar{s}\left(p_{\bar{b}}\right)$ and $\bar{q}\left(p_{\bar{b}}\right)$ predicted by (110) and (111), Δs and Δq are calculated from (16).

2.7.2 Numerical Scheme

We adopt a five cloud-type cumulus ensemble by choosing the values of λ_i listed in Table 1. All integrals over λ as well as all integrals over pressure, are performed by using the trapazoidal rule. The differential equations (48) and (51) are solved with a modified Euler predictor-corrector scheme.

Below the lowest level of detrainment, (67) and (68) are used in place of the equivalent expressions (34) and (35). This is done because the detrainment form of the equations, (67) and (68), appear to have computational advantages over (35) and (36) at the top of the transition layer and near cloud base. The finite difference scheme is forward in time with the eddy diffusion terms in (29) and (30) treated implicitly and all the vertical advective terms in (29), (30), (34), (35), (67), (68), (110), and (111) computed with upstream differences.

2.7.3 Large-Scale Condensation and Dry Convective Adjustment

The cumulus parameterization theory described in Section 2.3.2 accounts for subgrid scale condensation, evaporation, and precipitation which can occur when the atmosphere is not saturated in the large-scale sense. For generality, however, we must further account for large-scale moisture phase changes when the atmosphere becomes saturated across the entire model domain. To do this, the adjustment scheme of Hack and Schubert (1976) is implemented in the model. It turns out, however, that for the experiments reported here large-scale saturation is never achieved.

Similarly, if the potential temperature decreases with altitude in some region above p_b during the course of the integration, subgrid scale dry convection is assumed to occur such that a dry adiabatic lapse rate results there. This is accomplished by use of a dry convective adjustment scheme described by Hack and Schubert (1976). However, for the experiments described here, an unstable stratification requiring dry convective adjustment never occurs.

2.8 SUMMARY OF MODEL FORMULATION

A one-dimensional model of the tropical marine boundary layer has been proposed and, for convenience, will be summarized here.

2.8.1 The Surface Layer

A surface layer extending from the sea surface to a level indicated by p_a is assumed to exist in which the Monin-Obukhov Similarity Theory applies. This allows determination of the surface fluxes in terms of model-predicted quantities.

2.8.2 The Subcloud Mixed Layer

A subcloud mixed layer is assumed to exist extending from p_a to a level denoted by p_b in which $\bar{s}$ and $\bar{q}$ but not $\bar{u}$ and $\bar{v}$ are independent of altitude. Conservation equations for heat, moisture, mass, and momentum in this region are (26) through (30).

The subcloud mixed layer is topped by a stable transition layer which is modeled as a discontinuity in $\bar{s}$ and $\bar{q}$.

2.8.3 The Cloud Layer

A cloud layer in which $\bar{s}$, $\bar{q}$, $\bar{u}$, and $\bar{v}$ are all allowed to vary with altitude exists extending from p_b to the model top. All vertical subgrid scale fluxes of heat and moisture and all subgrid scale condensation and evaporation in this region are assumed to be accomplished by cumulus clouds that begin as updrafts originating from the mixed layer and have their bases just above p_b. These clouds are parameterized using the theory of Arakawa and Schubert (1974). Conservation equations for heat and moisture in this region are (34) and (35). The equations for the conservation of momentum in this region take the same form as (29).

2.8.4 Large-Scale Forcing Parameters

Because this is a one-dimensional study, $\bar{\omega}$, $\bar{u}_g$, $\bar{v}_g$, $\bar{\underline{v}}\cdot\overline{\nabla s}$, $\bar{\underline{v}}\cdot\overline{\nabla q}$, and $\bar{\underline{v}}_b\cdot\overline{\nabla p}_b$ must be imposed. In addition, since there is no upper ocean model involved, the SST must also be specified.

For all of the experiments reported here, we set $\bar{\underline{v}}\cdot\overline{\nabla q} = 0$ and $\bar{\underline{v}}\cdot\overline{\nabla p}_b = 0$. The thermal wind equation predicts $\overline{\nabla s}$ as a function of $\bar{u}_g$ and $\bar{v}_g$, and thus the imposed quantities which are regarded as large-scale forcing parameters in our experiments are $\bar{\omega}$, $\bar{u}_g$, $\bar{v}_g$, and the SST.

Section 3

DESCRIPTION OF THE EXPERIMENTS

We will model the undisturbed trade wind regime by finding quasi-steady solutions to the equations for various combinations of the imposed large-scale forcing parameters. The trade winds are particularly suited for this type of study because of their well-known steadiness.

Three sets of experiments are performed. Each set is accomplished by imposing $\bar{\omega}$, $\bar{u}_g$, $\bar{v}_g$, and the SST and integrating (26) through (30), (34) and (35) from arbitrary initial conditions to a quasi-steady state in which the thermodynamic variables change by only about 0.1% per hour. Then, with the same values for all the imposed parameters except the SST, the integration is repeated and other balanced states corresponding to various SST perturbations are found. The resulting differences in the thermodynamic structure of the atmosphere and the magnitude of the surface fluxes are then examined.

Five experiments are performed in each set with the SST varying by 0.25° K in the range from 301.5 to 302.5° K. The vertical profiles of $\bar{\omega}$ and $\bar{u}_g$ in the lowest 3 km for all three sets of experiments are shown in Figure 2 and Figure 3. The N-S component of the geostrophic wind is assumed to be independent of altitude and given by:

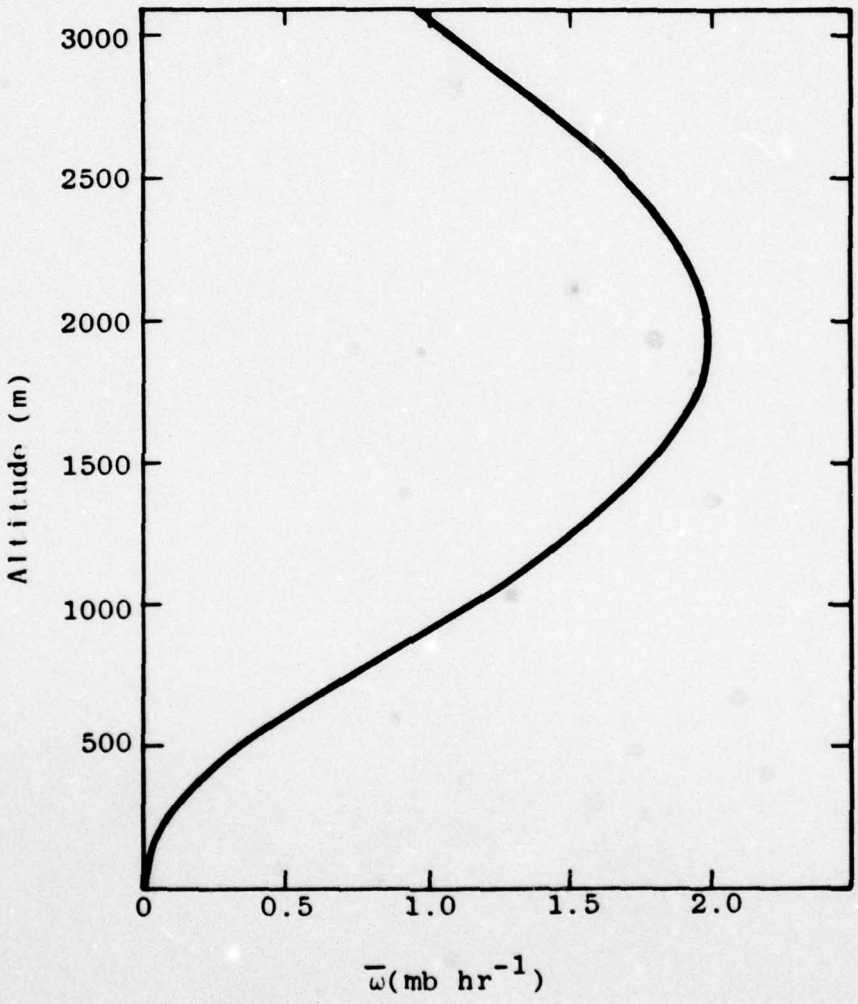

Figure 2. Vertical profile of the large-scale vertical p-velocity in the lower atmosphere for all three sets of experiments.

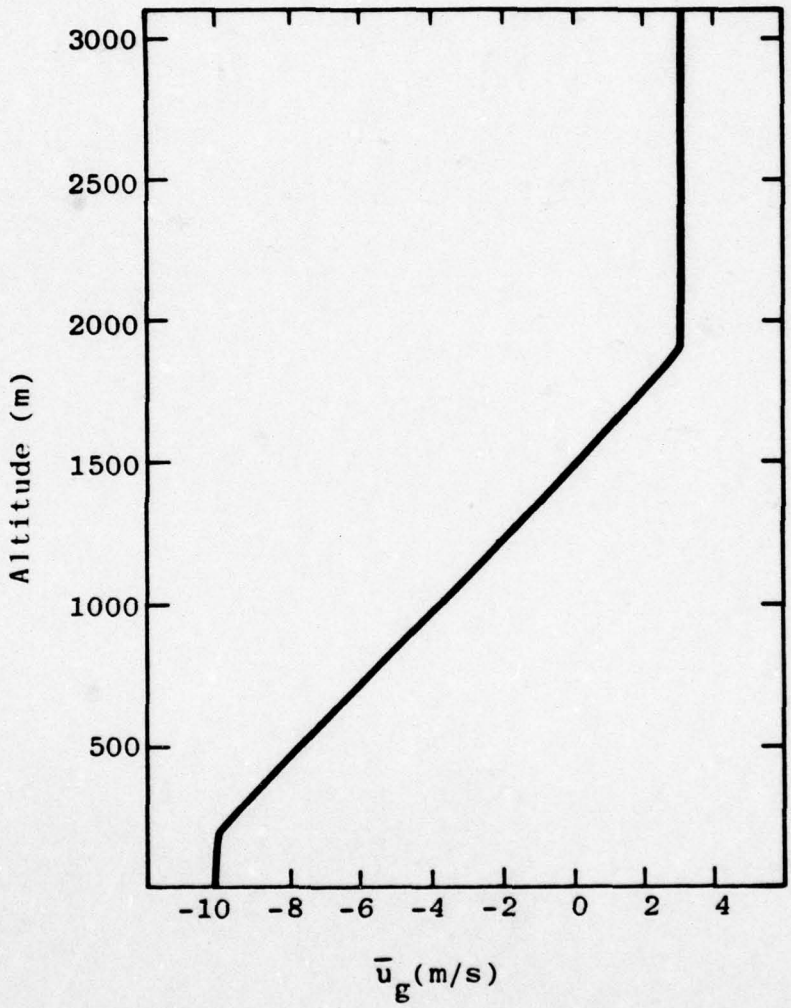

Figure 3. Vertical profile of the E-W component of the geostrophic wind for all three sets of experiments.

Experimental Set	$\bar{v}_g$
1	$-2.0\ m\ s^{-1}$
2	$-2.5\ m\ s^{-1}$
3	$-3.0\ m\ s^{-1}$

Model constants for all experiments are given in Table 1.

The imposed parameters for these experiments are fairly representative of the average situation in the undisturbed summertime Western Atlantic Trades. Note also that, consistent with the assumed profile of $\bar{u}_g$ and the thermal wind equation, increasing $|\bar{v}_g|$ increases the cooling rate in the lower atmosphere due to horizontal advection. Thus, the advective cooling of the marine boundary layer increases from experimental set 1 to set 3.

Section 4

RESULTS

Figure 4 shows the vertical profile of potential temperature resulting from an integration in experimental set 1 with a SST of 302.0 ^{o}K. The layered structure of the marine boundary layer discussed earlier is clearly evident with the trade inversion at about 1700 m hiehgt and the top of the mixed layer at about 500 m height. Consistent with the diagnostic studies alluded to in Section 1, the clouds are confined below the top of the trade inversion and the compressional heating in the inversion due to large-scale subsidence is balanced by the evaporative cooling of detrained cloud droplets. In the cloud layer below the base of the inversion, the main balance is between the cooling due to radiation and horizontal advection and the warming due to cumulus-induced subsidence. In the mixed layer the warming caused by the surface and entrainment fluxes of heat is balanced by the cooling due to radiation and horizontal advection.

Figure 5 shows the vertical profile of water vapor mixing ratio for the same experiment. The layered structure is again evident and in this case the drying effect of the large-scale subsidence in the trade inversion is balanced by the detrainment of both liquid water and water vapor. Note that Figure 5 indicates $\partial\bar{q}/\partial p = 0$ in the lower part of the cloud layer. This is because all of the clouds have their tops in the trade inversion. Thus, the detrainment rate, D(p), is zero in

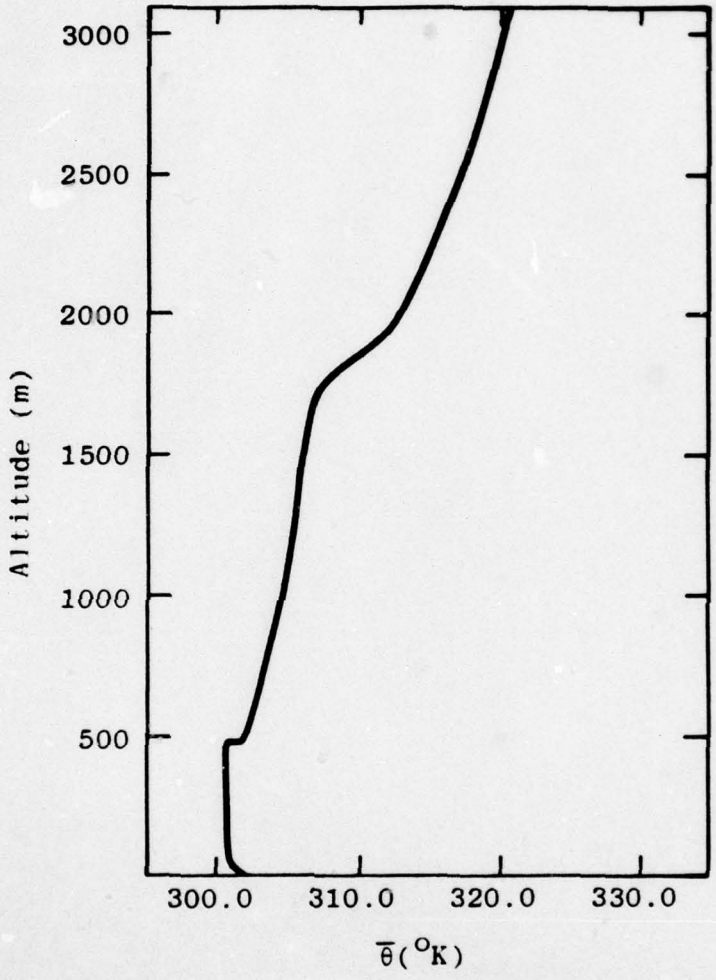

Figure 4. Vertical profile of potential temperature in the lower atmosphere for experimental set 1, SST = 302.0 K.

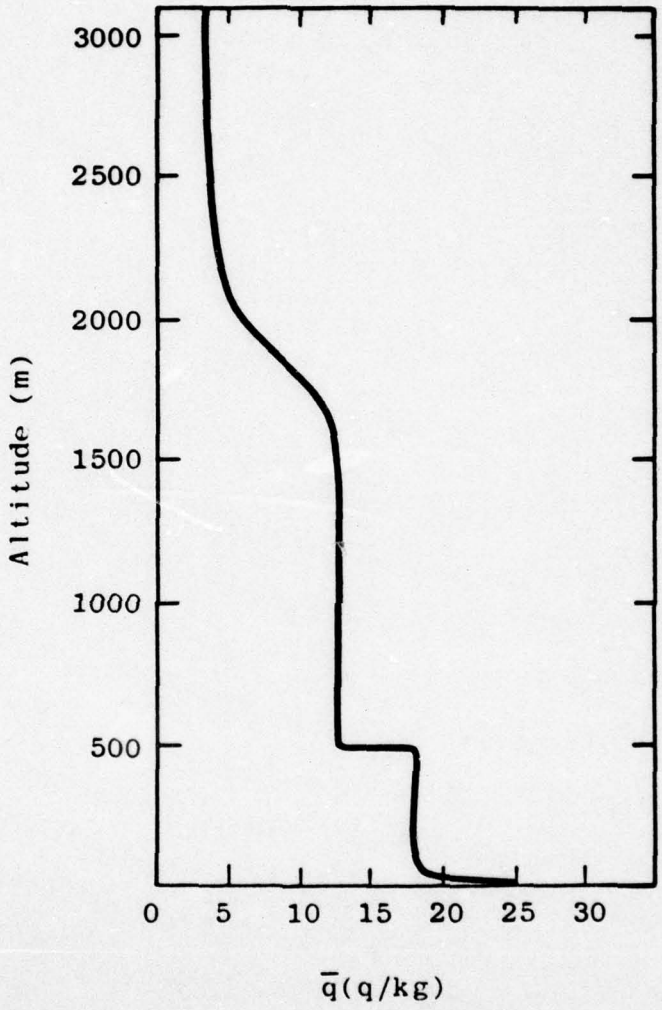

Figure 5. Vertical profile of water vapor mixing ratio in the lower atmosphere for experimental set 1, SST = 302.0 K.

the lower part of the cloud layer, which from (68) requires $\partial\overline{q}/\partial p = 0$ there in the steady state since $\overline{\underline{v}}\cdot\overline{\nabla q}$ is assumed zero. In the mixed layer, the surface evaporation is balanced by the entrainment flux at p_b.

Figure 6 shows the vertical profiles of $\overline{u}$ and $\overline{v}$ for the same experiment. In the free atmosphere the wind remains near its geostrophic value while an Ekman balance exists in the mixed layer where the eddy viscosity is significant. Thus in the mixed layer, as expected, the wind vector is smaller in magnitude than, and directed to the left of, the geostrophic wind vector.

Consistent with the diagnostic studies mentioned in Section 1, the cumulus-induced subsidence in the environment at the top of the mixed layer, $-\left(\overline{\omega}_\sigma\right)_b$ is more than an order of magnitude larger than the large-scale subsidence there, $\overline{\omega}_b$ (see equation (8)). Thus, in the steady state, the deepening rate of the mixed layer caused by entrainment at its top is balanced essentially by this cumulus induced subsidence.

The physical balances responsible for maintaining the vertical structures of the marine boundary layers as well as the vertical structures themselves for the other experiments, are qualitatively similar to the case just described and will not be discussed here. Instead, we will examine relationships among the cloud mass flux, the mixed layer thermodynamic variables, the surface fluxes, and the sea surface temperature.

Figure 7 shows the percent cloud cover, assumed proportional to the total cloud base mass flux according

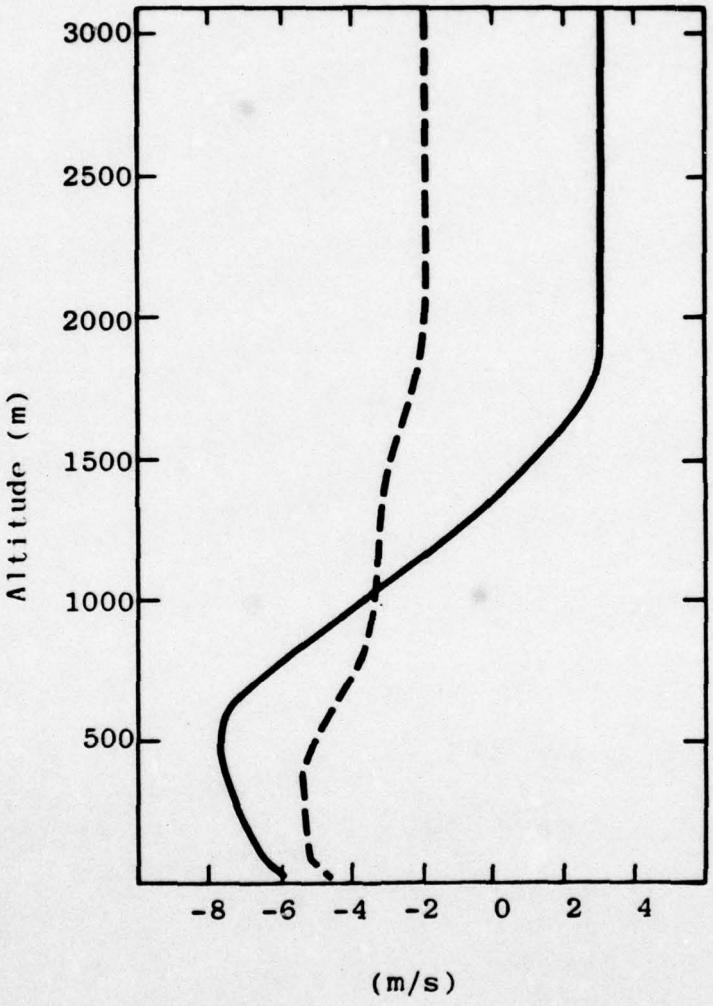

Figure 6. Vertical profiles of $\bar{u}$(——) and $\bar{v}$(----) in the lower atmosphere for experimental set 1, SST = 302.0 K.

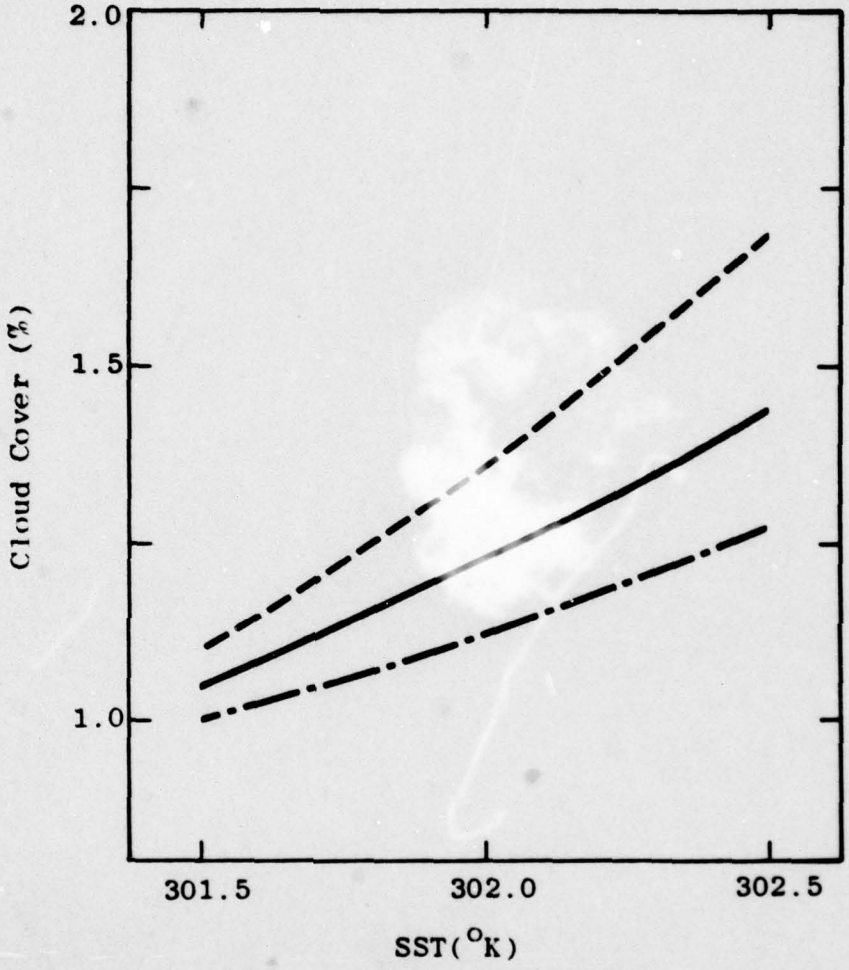

Figure 7. Percent cloud cover as a function of SST for (a) experimental set 1 (— - —), (b) experimental set 2 (————), and (c) experimental set 3 (- - - -).

to (66), as a function of SST for the three sets of experiments. As expected, increasing the SST increases the cloud cover. Furthermore, the cloud cover is a weakly nonlinear function of SST with the rate of increase becoming larger at higher SST's. Figure 7 also indicates that the cloud cover at a particular SST increases from set 1 to set 3. This is because more vigorous cumulus convection is required to balance the greater advective cooling in the cloud layer as the southward somponent of the geostrophic wind is made more negative.

Figure 8 shows mixed layer portential temperature for the three sets of experiments as a function of SST. Note that it shows little variation from set 1 to set 3 and increases linearly with the SST in all cases with a slope of about 1.1. Figure 9, on the other hand, indicates a quite different behavior for the mixed layer water vapor mixing ratio which decreases significantly as $|\bar{v}_g|$ increases and shows a weakly nonlinear decrease with SST. The results indicate, however, that the average moisture content of the entire marine boundary layer increases with the SST, implying that the cloud layer becomes more moist as the SST increases. Furthermore, this increase is approximately linear with a slope of about 0.5 g kg^{-1} $^{o}K^{-1}$.

The net heat flux at the sea surface, E_o, can be written

$$E_o = H_o + L_v Q_o + F_o^* + S_o^* \quad ,$$

where H_o is the surface sensible heat flux (calculated from (82)), $L_v Q_o$ the surface latent heat flux (calculated from (83)), F_o^* the surface long-wave radiative flux

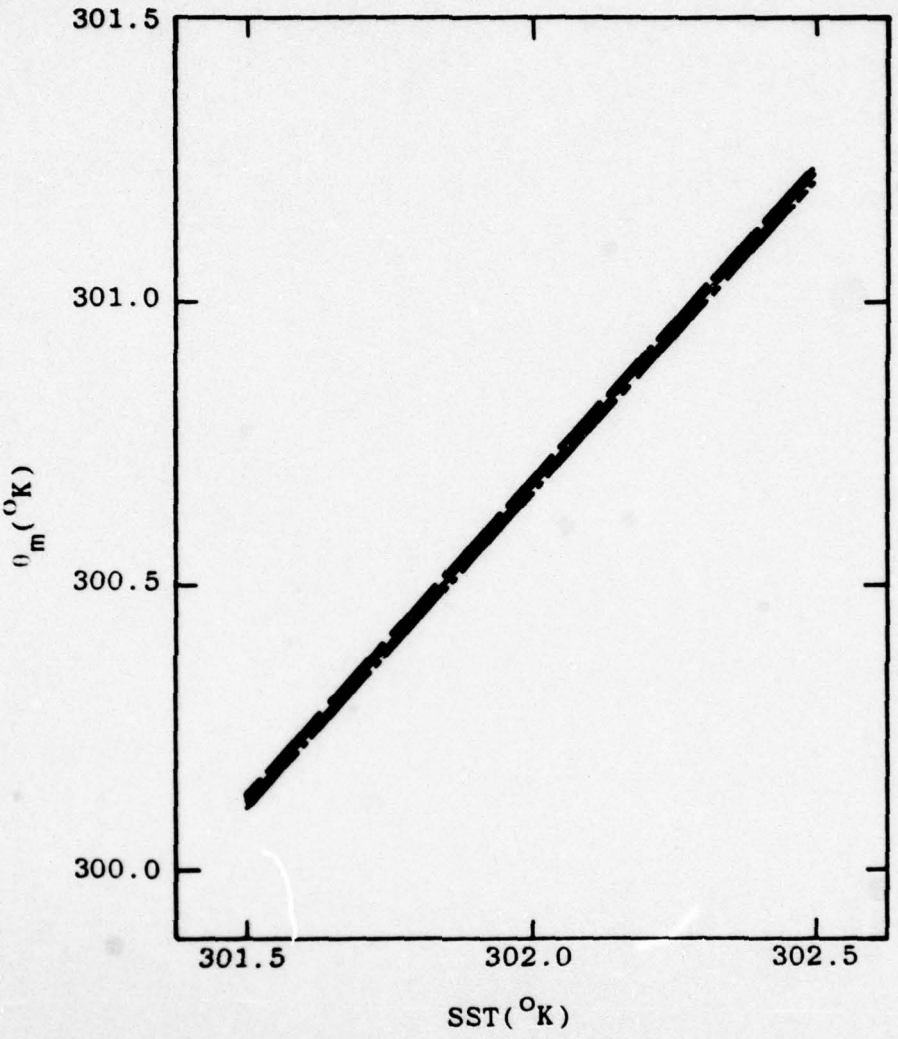

Figure 8. Mixed layer potential temperature as a function of SST for (a) experimental set 1 (— - —), (b) experimental set 2 (————), and (c) experimental set 3 (—— ——).

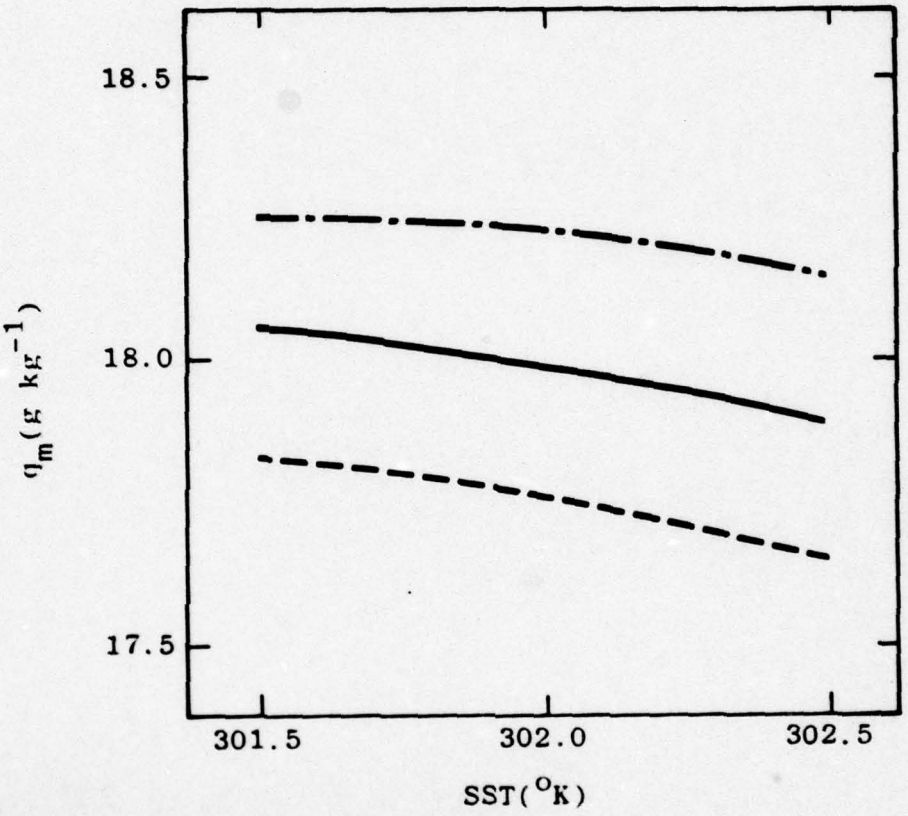

Figure 9. Mixed layer water vapor mixing ratio as a function of SST for (a) experimental set 1 (— - —), (b) experimental set 2 (————), and (c) experimental set 3 (— — —).

(calculated from (96)), and S_o^* the surface short-wave radiative flux (calculated from (102)). Figures 10 through 12 show these quantities as a function of SST for the three sets of experiments. Note that H_o, F_o^*, and S_o^* show almost no variation from set 1 to set 3 and are practically independent of SST for the range considered. The magnitude of the surface latent heat flux, however, increases from set 1 to set 3 and varies linearly with the SST for all three sets with a slope of approximately -105 cal cm^{-2} day^{-1} $^oK^{-1}$. Thus, essentially all of the variation of E_o is due to the latent heat flux and we find dE_o/dT_o about 1.6 times the value estimated by Bathan et al. (1976) and about 1.1 times the value estimated by Piacsek et al. (1976).

Figure 13 shows the surface latent heat flux plotted against percent cloud cover for an SST of 302.5° K. The increase of the surface evaporation rate with increasing cloud cover indicated by Figure 13 is consistent with the findings of Ogura and Cho (1973) who studies the interaction between the subcloud and cloud layers with a simple analytical model. This relationship between cloud activity and surface evaporation rate implies that cumulus convection must be treated adequately in any model used to predict the surface latent heat flux since feedback between the surface evaporation and the cumulus convection can amplify dQ_o/dT_o. The neglect of cumulus convection by Clancy (1977) may be the reason for the unreasonably small value of dE_o/dT_o predicted by that study.

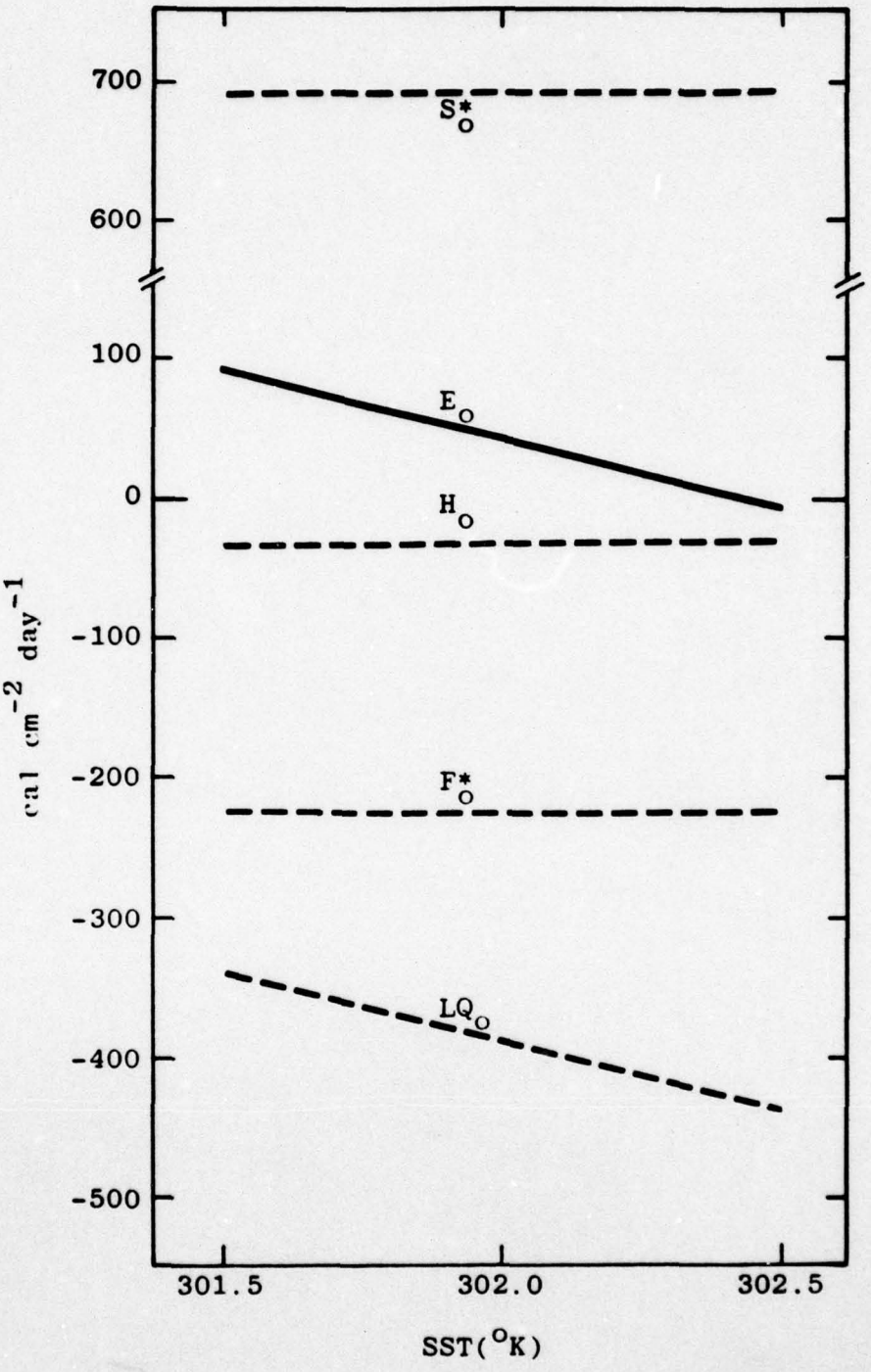

Figure 10. Surface heat fluxes (positive downward) as a function of SST for experimental set 1. The total flux E_o is the algebraic sum of the solar flux S^*_o, the long-wave flux F^*_o, the sensible heat flux H_o, and the evaporative heat flux.

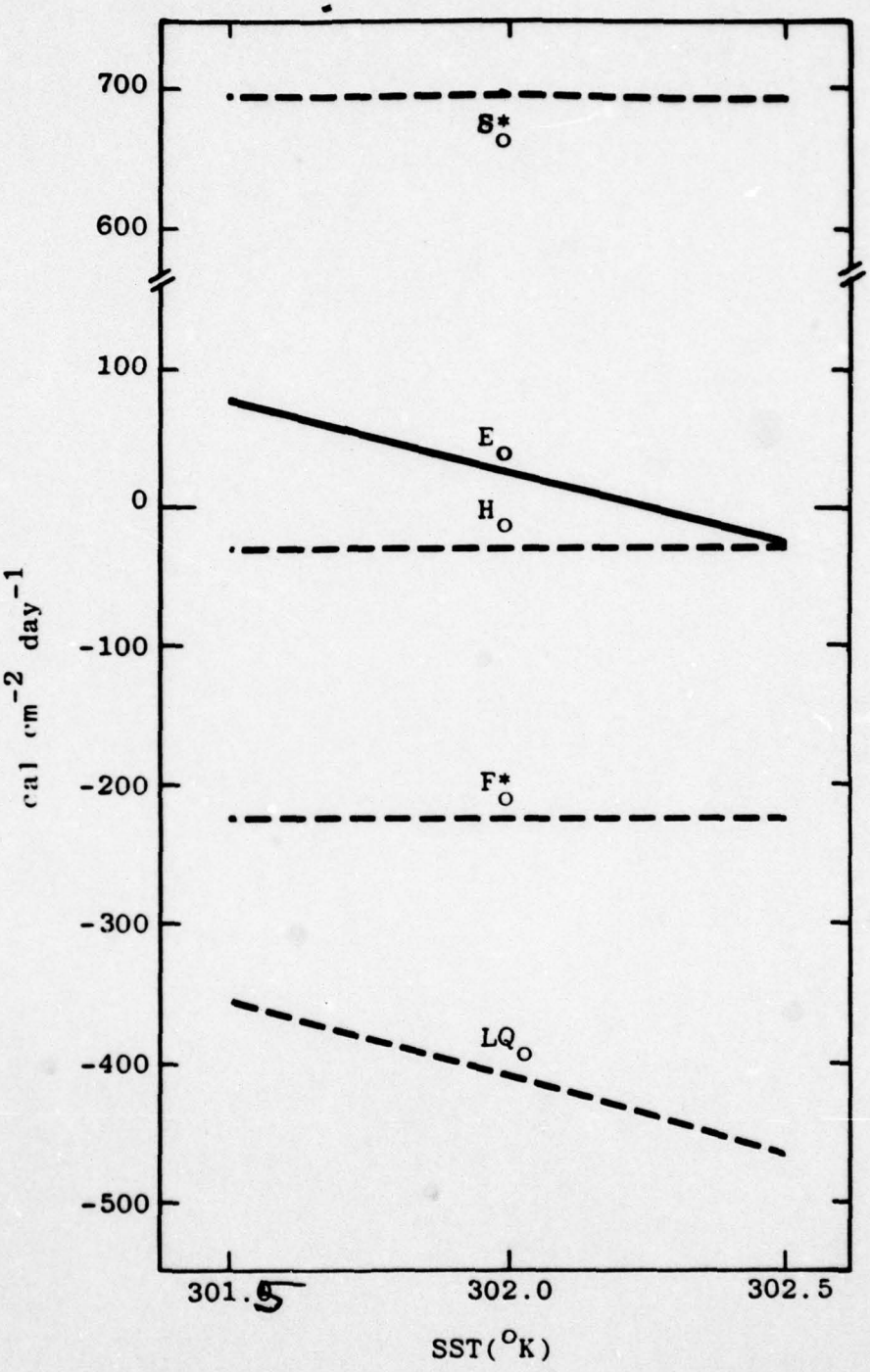

Figure 11. Surface fluxes (positive downward) as a function of SST for experimental set 2.

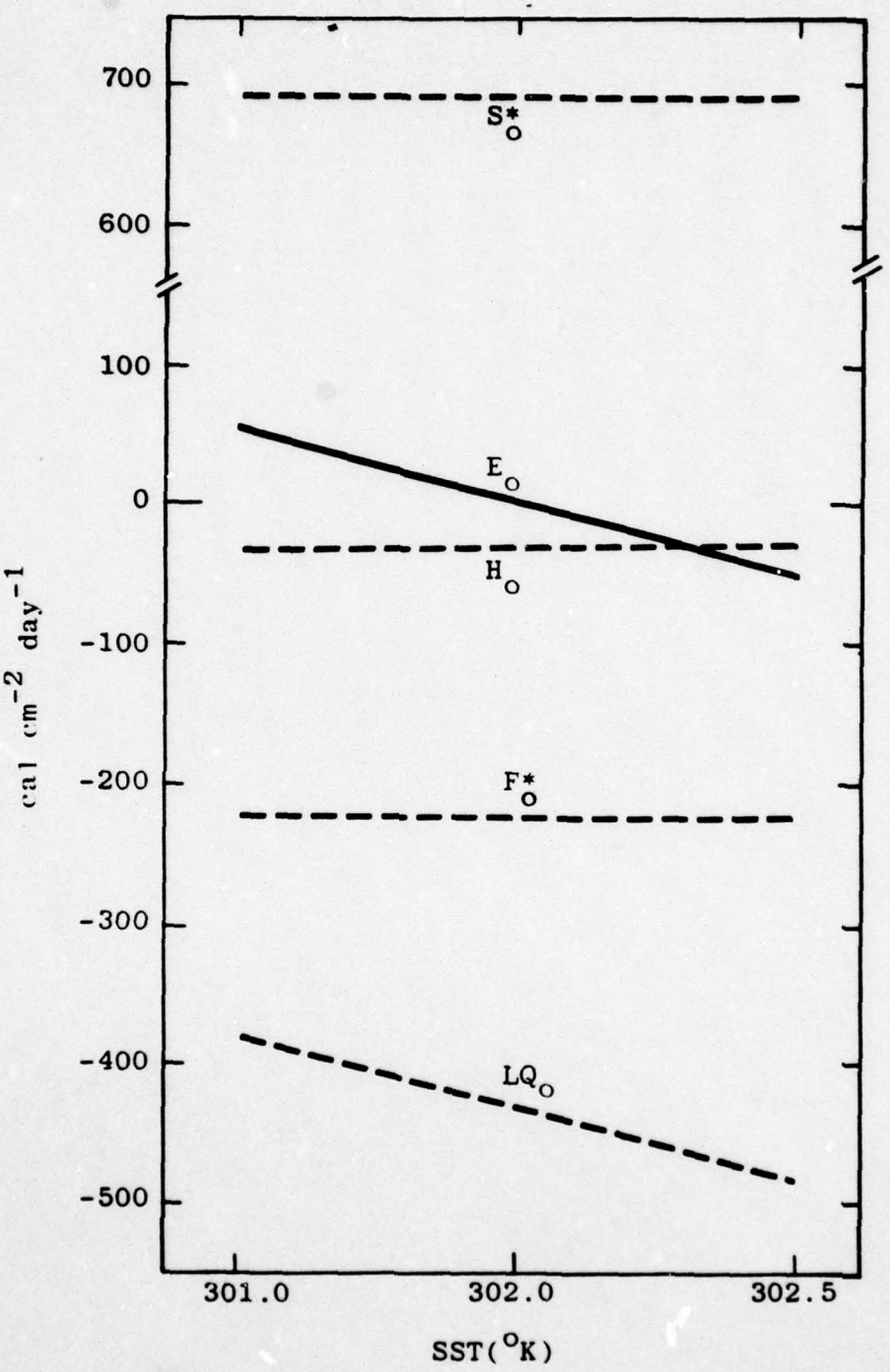

Figure 12. Surface fluxes (positive downward) as a function of SST for experimental set 3.

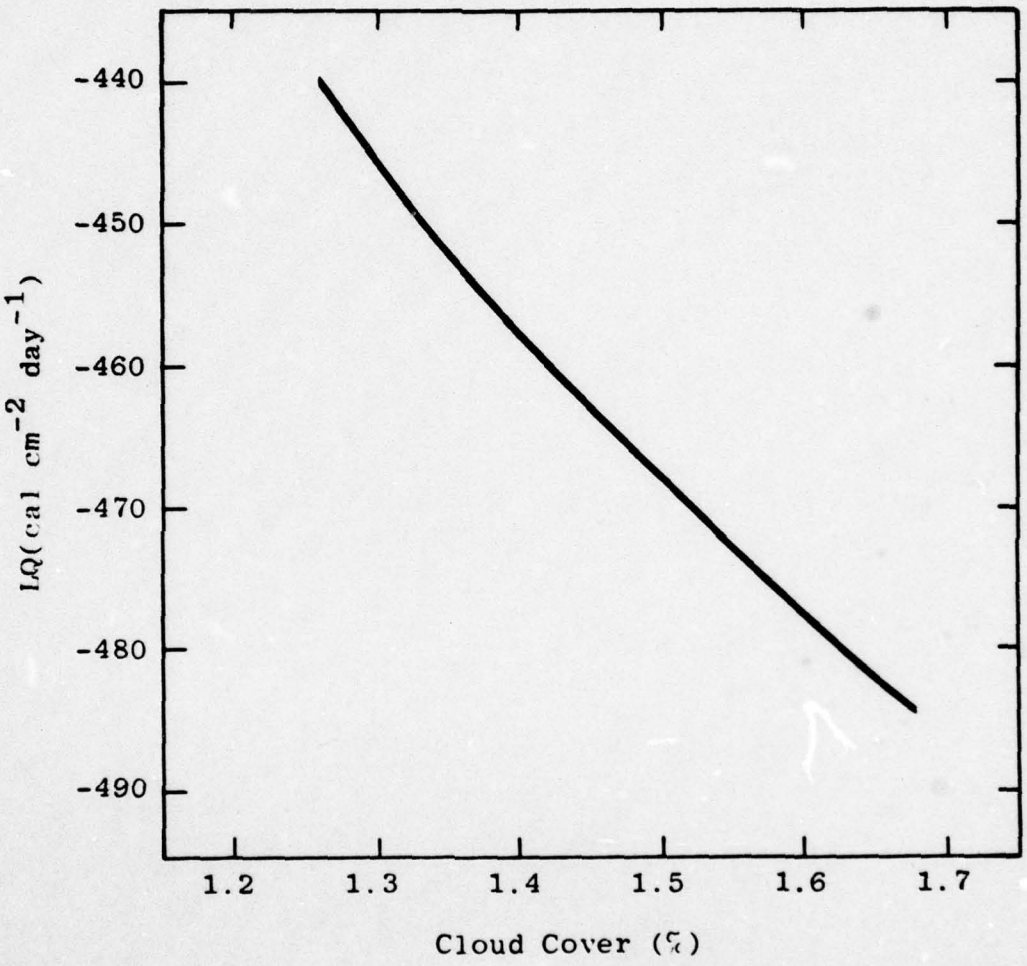

Figure 13. Surface latent heat flux (positive downward) as a function of percent cloud cover for a sea surface temperature of 302.5 K.

Section 5

SUMMARY AND DISCUSSION

A one-dimensional numerical model of the tropical atmosphere has been constructed and used to investigate the effect of sea surface temperature perturbations in the range likely to be generated by Ocean Thermal Power Plants on the marine boundary layer of the summertime Western Atlantic trade wind regime. Conservation equations for heat, moisture, and momentum are solved on a vertically stretched grid extending from the sea surface to about tropopause level. Vertical eddy fluxes of heat and moisture above the surface layer are accounted for by the theory of Arakawa and Schubert (1974). In the subcloud mixed layer the vertical eddy flux of momentum is modeled with the eddy diffusion coefficient representation of O'Brien (1970). In the surface layer the eddy fluxes of heat, moisture, and momentum are determined from the Monin-Obukhov similarity theory. The flux of long-wave radiation is treated with the formulation of Danard (1969), while the short-wave radiative flux is calculated from the model of Arakawa, Katayama, and Mintz (1968).

Vertical profiles of the large-scale vertical p-velocity and the geostrophic wind are imposed along with the SST, surface pressure, and boundary conditions for the prognostic variables. The horizontal gradient of moisture is assumed zero while the horizontal gradient of temperature is implied from the imposed geostrophic wind profile. Thus, the horizontal advection of moisture is ignored but the horizontal advection of heat is included in a self-consistent fashion.

The model is integrated from arbitrary initial conditions to a quasi-steady state. Then, for various combinations of the imposed parameters, the integration is repeated and other quasi-steady states are found. The influences of SST and cloud cover (which is assumed proportional to the total cloud base mass flux) on the structure of the marine boundary layer and the magnitude of the surface fluxes are then examined.

The height of the trade wind inversion and the thickness of the atmospheric mixed layer are not appreciably affected by changes of SST of 1 ^{o}C. In addition, the surface fluxes of long-wave radiation, short-wave radiation, and sensible heat are found to be little affected by small changes in SST and cloud cover. The surface latent heat flux (taken positive downward), however, varies linearly with the SST with a slope of about -105 cal cm^{-2} day^{-1} ^{o}K^{-1} and accounts for practically all of the variation of the net surface heat flux with respect to SST. The surface evaporation is found to increase with increasing cloud cover at a fixed SST, but its variation with respect to SST is independent of small changes in the cloud cover. In addition, the cloud cover increases with SST if all other imposed parameters are the same.

From the standpoint of OTPP influence on regional climate, the change induced in the surface evaporation rate is the most significant quantity since it is probably well correlated with rainfall. The present study indicates that the surface evaporation rate changes substantially with the SST and, consequently, must be given proper consideration when planning the deployment of OTPP's. For example, if

the maximum tolerable change in the surface evaporation rate is taken to be -5%, we find that maximum allowable SST perturbation is about -0.2^{o} C.

The present study can be extended in several ways. First of all, the cumulus parameterization model can be improved by dropping the assumption that the cloud updrafts begin with the mixed layer values of dry static energy and water vapor mixing ratio (see Equations (55) and (56)). Rather, following Ogura and Cho (1974), we can recognize the fact that updrafts in the mixed layer which ultimately produce cumulus clouds tend to be slightly warmer and more moist than their surroundings. This will allow the existence of cloud-induced eddy fluxes of heat and moisture out of the mixed layer. Note that these eddy fluxes do not occur in the present model since the rates at which heat and moisture are transported out of the mixed layer into rising cumulus clouds are exactly balanced by the rates at which these quantities are put back into the mixed layer by compensating subsidence in the environment.

In addition, the case of saturated mixed layers should be accounted for. Recall that the present study applies only to the tupical trade wind situation in which cloud base is slightly above the top of the mixed layer. This gives rise to scattered trade wind cumuli which are accounted for by the Arakawa-Schubert theory. As discussed by Schubert (1976), however, cloud base often falls below the top of the mixed layer in subtropical latitudes. In this case a solid deck of stratocumulus clouds exists in the upper part of the mixed layer and must be accounted for by another theory. This could be extremely important to the OTPP problem. For example, if OTPP operation causes a

transition from the scattered cumuli regime to the stratocumulus regime, the surface radiative fluxes may be altered drastically. Unfortunately there is at present no adequate theory for the transition from an unsaturated to a saturated mixed layer. However, a forthcoming paper by Randall and Arakawa (1978) should be helpful in this regard.

A more serious drawback of the present study is that it treats the ocean as an infinite heat reservoir and ignores the highly interactive nature of the upper ocean and lower atmosphere. A more realistic approach would be to couple the marine boundary layer model described here to an appropriate upper ocean model. Then, OTPP's could be treated as diabatic heat sinks and the coupled model could be used to predict the resulting equilibrium SST and the surface fluxes for various degrees of OTPP activity.

A coupled model as envisioned above would, of course, be useful in air-sea interaction studies other than those related to the OTPP problem. One possible application of such a sophisticated model would be to test the validity of simpler models linking the ocean and atmosphere for the purpose of atmospheric and/or oceanic forecasting.

A coupled air-sea model of this type should eventually be extended to two dimensions. This would allow an explicit treatment of horizontal advection and the characteristics of the atmosphere downstream from the OTPP-generated SST anomaly could be examined. In addition, the large-scale vertical motion and one component of the geostrophic wind could be predicted rather than prescribed, thereby allowing the SST anomaly to alter the large-scale flow pattern.

Appendix A

LIST OF SYMBOLS

$A(\lambda)$	Cloud work function for subensemble λ.
$A_{LS}(\lambda)$	Cloud work function for subensemble λ generated by large-scale processes alone in one time step of the model.
a_o	Albedo of air column from sea surface to model top.
a_s	Albedo of sea surface.
B	Stefan-Boltzman constant.
c	Total condensation rate per unit mass of air.
c_p	Specific heat at constant pressure for dry air.
C_o	Raindrop generation rate parameter.
$c(\lambda,p)$	Condensation rate for subensemble λ at level p per unit cloud mass flux.
$D(p)$	Total detrainment rate for the cloud ensemble at level p.
e	Total evaporation rate per unit mass of air.
E_o	Net heat flux at the sea surface (positive downward).
dE_o/dT_o	Change in the net surface heat flux with respect to sea surface temperature.
f	Coriolis parameter.
$F(\lambda)$	Large-scale forcing for subensemble λ.
F^*_{CLR}, F^*_{CLD}	Net downward flux of long-wave (infrared) radiation in clear region, cloudy region.
F^*_o	Net downward flux of long-wave (infrared) radiation at sea surface.

g	Acceleration of gravity.
$\bar{H}$	Atmospheric scale height, $R\bar{T}/g$.
h	Moist static energy.
h^*	Saturated moist static energy.
$h_\sigma(\lambda,p)$	Moist static energy of clouds in subensemble λ at level p.
H_o	Surface sensible heat flux (positive downward)
k	Entrainment parameter
K^*	Vertical eddy diffusion coefficient for momentum.
$K(\lambda,\lambda')$	Kernel from cumulus parameterization theory.
$K_V(\lambda,\lambda')$	Vertical mass flux kernel.
$K_D(\lambda,\lambda')$	Detrainment kernel.
$K_M(\lambda)$	Mixed layer kernel.
L_v	Latent heat of evaporation for water.
L	Monin-Obukhov length.
$\ell(\lambda,p)$	Liquid water mixing ratio of clouds in subensemble λ at level p (mass of liquid water per mass of dry air).
$\hat{\ell}(p)$	Liquid water mixing ratio of cloud air detrained at level p.
L_vQ_o	Surface latent heat flux (positive downward).
$m_b(\lambda)\ d\lambda$	Vertical mass flux (positive upward) at p_b for subensemble λ.
N	Total number of clouds in cumulus ensemble.
OTPP	Ocean Thermal Power Plant.
p, p_r	Pressure, reference pressure.
p_o, p_1, p_a	Pressure at surface, first gridpoint above surface, top of surface layer.

p_b, $p_{\overline{b}}$, p_c	Pressure at top of mixed layer, top of transition layer, cloud base.
$p_d(\lambda)$	Pressure at level of detrainment (level of cloud tops) for clouds in subensemble λ.
p_e	Pressure at model top.
$\overline{Q}_R$	Net radiational heating rate.
q	Water vapor mixing ratio (mass of water vapor per mass of dry air).
q_m	Horizontally-averaged water vapor mixing ratic of mixed layer.
$q_\sigma(\lambda,p)$	Water vapor mixing ratio of clouds in subensemble λ at level p.
q^*	Saturation value of water vapor mixing ratio.
$\hat{q}(p)$	Water vapor mixing ratio of cloud air
q_o, q_{10}	Water vapor mixing ratio at sea surface, 10 m height.
$-Q_o$	Surface evaporation rate.
R	Gas constant for dry air.
R^*	Total raindrop generation rate per unit mass of air.
$r(\lambda,p)$	Raindrop generation rate for subensemble λ at level p per unit cloud mass flux.
s	Dry static energy.
s_m	Horixontally-averaged dry static energy of mixed layer.
s_v	Virtual dry static energy.
$s_\sigma(\lambda,p)$	Dry static energy of clouds in subensemble λ at level p.
$s_{v\sigma}(\lambda,p)$	Virtual dry static energy of clouds in subensemble λ at level p.

$\hat{s}(p)$	Dry static energy of cloud air detrained at level p.
S_o	Incident short-wave (solar) radiation at model top.
S_o^S	Downward flux of short-wave radiation subject to scattering.
S_o^A	Downward flux of short-wave radiation subject to absorption.
$s(p)$	Dry static energy of cloud air detrained at level p.
S^*_{CLR}, S^*_{CLD}	Net downward flux of short-wave (solar) radiation in clear region, cloudy region.
S^*_o	Net downward flux of short-wave (solar) radiation at sea surface.
SST	Sea Surface Temperature.
t	Time.
T, T_r	Temperature, reference temperature
T_o	Temperature at sea surface.
u	Component of wind in x-direction
u_g	Component of geostrophic wind in x-direction.
u_*	Surface atmospheric friction velocity.
U, U_1	Wind speed, wind speed at first gridpoint above sea surface.
U_o	Wind speed at sea surface.
v	Component of wind in y-direction.
v_g	Component of geostrophic wind in y-direction.
$\underset{\rightarrow}{v}$	Wind velocity vector on a surface of constant pressure.
$\underset{\rightarrow}{v}_{og}$	Geostrophic wind velocity vector at sea surface.

$\underline{v}_c$	Mean current vector in upper layer of ocean.
w_b	Average vertical velocity of updrafts entering clouds at p_b.
$w(p)$	Pressure corrected precipitable water vapor.
x, y, z	Tangent plane Cartesian coordinates; x positive eastward, y positive northward, z positive upward from the sea surface.
z_o	Surface roughness length.
z_1	Altitude of first gridpoint above sea surface.
α	Solar zenith angle
γ	$\frac{L_v}{c_p}\left(\frac{\partial q^*}{\partial T}\right)_p$
δ	Solar declination angle.
ε	Flux emissivity of pure water vapor.
ε'	Derivative of flux emissivity with respect to pressure corrected precipitable water vapor.
ε_o	Emissivity of sea surface.
θ	Potential temperature.
θ_o	Potential temperature at sea surface.
θ_m	Horizontally-averaged potential temperature of mixed layer.
ϕ	Latitude.
$\phi_\theta, \phi_q, \phi_m$	Non-dimensional vertical derivative of temperature, water vapor mixing ratio, wind speed in surface layer.
ρ	Density of moist air.
ρ_a, ρ_w	Reference density for air, water.
ρ_b	Density of air at p_b.
σ	Fraction of model domain covered by clouds.

σ_i	Fraction of model domain covered by i-th cloud.
κ	von Karmen's constant.
λ	Entrainment rate for clouds in subensemble .
$\lambda_d(p)$	Entrainment rate for clouds that have level of detrainment (level of cloud tops) at level p.
$n(\lambda,p)$	Ratio of vertical mass flux due to subensemble λ at level p to vertical mass flux due to subensemble λ at p_b.
ω	Vertical p-velocity, dp/dt.
$\overline{\omega}_\sigma$	Average vertical p-velocity in cloud ensemble times fraction of model domain covered by the ensemble.
$\overline{\omega}_\sigma(\lambda,p)$	Average vertical p-velocity in type λ clouds at level p times fraction of model domain covered by subensemble .
$\overline{\omega}_{\sigma\ b}$	Average vertical p-velocity in cloud ensemble at p_b times fraction of model domain covered by the ensemble.
$\overline{\omega}_b$	Vertical p-velocity at p_b averaged across entire model domain.
$\tilde{\omega}_b$	Vertical p-velocity at p_b averaged across part of model domain not occupied by clouds.
$\vec{\tau}_o$	Surface wind stress vector.
τ_o^x, τ_o^y	Component of surface wind stress vector in x-direction, y-direction.
Δt	Time step in numerical integration.
Δs	Jump of dry static energy across transition layer.
Δq	Jump of water vapor mixing ratio across transition layer.
Δs_v	Jump of virtual dry static energy across transition layer.

$\hat{i}$, $\hat{j}$	Unit vector in x-direction, y-direction.
(∇)	Gradient operator at constant pressure.
$(\bar{\ })$	Horizontal average on constant pressure surface taken across entire model domain.
$(\tilde{\ })$	Horizontal average on constant pressure surface taken across part of model domain not occupied by clouds.
$(')$	Deviation from horizontal average taken across entire model domain.
$(\ )_M$	Average taken over depth of mixed layer.
$(\overline{\omega' s'})_o$, $(\overline{\omega' s'})_b$	Vertical eddy flux of dry static energy at surface, p_b.
$(\overline{\omega' q'})_o$, $(\overline{\omega' q'})_b$	Vertical eddy flux water vapor mixing ratio at surface, p_b.
$(\overline{\omega' s_v'})_o$, $(\overline{\omega' s_v'})_b$	Vertical eddy flux of virtual dry static energy at surface, p_b.
$(\overline{\omega' s'})_\sigma$, $(\overline{\omega' q'})_\sigma$, $(\overline{\omega' \ell'})_\sigma$	Total vertical cloud-induced flux of dry static energy, water vapor mixing ratio, liquid water mixing ratio.

Appendix B

DETERMINATION OF SATURATION MIXING RATIO AND GAMMA

By definition, the saturation mixing ratio, q^*, is given by

$$q^*(T,p) = \frac{0.622\ e_s(T)}{p - e_s(T)} \quad , \tag{B.1}$$

where $e_s(T)$ is the saturation vapor pressure over a plane surface of water. Following Washington and Kasahara (1970), we take

$$e_s(T) = 6.11 \exp\left[\frac{17.269(T - 273.16)}{T - 35.86}\right] , \tag{B.2}$$

where $e_s(T)$ is in mb and T is in degrees Kelvin.

The function γ is defined by

$$\gamma(T,p) = \frac{L_v}{c_p}\left(\frac{\partial q^*}{\partial T}\right)_p \quad . \tag{B.3}$$

Using (B.1) and (B.2), (B.3) can be written

$$\gamma(T,p) = 4098\ \frac{L_v}{c_p}\ \frac{p}{(p - e_s(T))}\ \frac{q^*(T,p)}{(T - 35.86)^2} \ . \tag{B.4}$$

Appendix C

SOLUTION OF THE FREDHOLM INTEGRAL EQUATION

The discrete representation of (65) is

$$G(\lambda_i) = \sum_{j=1}^{m} \left\{ K_{i,j}\, m_j\, Q_j\, \Delta\lambda \right\} + \frac{A_{LS}\, \lambda_i}{\Delta t} = 0$$

$$\text{for } i = 1,2,\ldots,n \quad , \tag{C.1}$$

where Q_j depends on the quadrature formula used. $\Delta\lambda = \lambda_{j+1} - \lambda_j$, and n is the number of cloud types represented in the model. An iterative scheme for solving (C.1) is

$$\frac{\partial m_i}{\partial \nu} = G(\lambda_i) \quad , \tag{C.2}$$

where Δ is an acceleration factor. Equation (C.2) can be written in fully implicit form as a matrix equation

$$\frac{m^{(k+1)} - m^{(k)}}{\Delta\nu} = \frac{D}{2}\left[m^{(k)} + m^{(k+1)} \right] + \frac{A_{LS}}{\Delta t} \quad , \tag{C.3}$$

where

$$D = K_{i,j}\, Q_j\, \Delta\lambda \quad ,$$

and k is an iteration index.

Equation (C.3) can be rearranged to give

$$m^{(k+1)} = E\left[\frac{A_{LS}}{\Delta t} + \frac{D}{2}\, m^{(k)} + \frac{m^{(k)}}{\Delta \nu}\right] \quad , \qquad (C.4)$$

where

$$E = \left[\frac{I}{\Delta \nu} - \frac{D}{2}\right]^{-1} \quad ,$$

and I is the identity matrix. Equation (C.4) is solved iteratively for the elements of m which yield the best solution of (C.1) subject to the constraints of (65).

REFERENCES

1. Arakawa, A., 1971, "A Parameterization of Cumulus Convection and its Application to Numerical Simulation of the Tropical General Circulation", presented at the 7th Tech. Conf. Hurricanes and Tropical Meteorology, Barbados, Amer. Meteor. Soc.

2. Arakawa, A., A. Katayama and Y. Mintz, 1968, "Numerical Simulation of the General Circulation of the Atmosphere", Proc. WMO (IUGG Symp. National Weather Prediction), Tokyo.

3. Arakawa, A. and W.H. Schubert, 1974, "Interaction of a Cumulus Cloud Ensemble with the Large-Scale Environment, Part I", J. Atmos. Sci., 31, 674-701.

4. Bathen, K.H., et al., 1976, "A Further Evaluation of the Oceanographic Conditions off Keahole Point, Hawaii, and the Environmental Impact of Nearshore OTEC Plants on Subtropical Hawaiian Waters", final report, Department of Ocean Engineering, Univ. of Hawaii.

5. Ball, F.K., 1960, "Control of Inversion Height by Surface Heating", Quart. J. Roy. Meteor. Soc., 86, 483-494.

6. Betts, A.K., 1973, "Nonprecipitating Cumulus Convection and its Parameterization", Quart. J. Roy. Meteor. Soc., 99, 178-196.

7. Bunker, A.F., B. Haurwitz, J.S. Malkus and H. Stommel, 1949, "Vertical Distribution of Temperature and Humidity over the Caribbean Sea", Papers Phys. Oceanogr. Meteor., 11, 81 pp.

8. Busch, N.E., 1977, "Fluxes in the Surface Boundary Layer over the Sea", Chapt. 6, Modeling and Prediction of the Upper Layers of the Ocean, Pergamon Press, New York.

AD-A067 510 SCIENCE APPLICATIONS INC MCLEAN VA OCEAN SCIENCE DIV F/G 8/10
A NUMERICAL MODEL OF THE TROPICAL MARINE BOUNDARY LAYER FOR ASS--ETC(U)
MAR 78 R M CLANCY N00173-77-C-0033
UNCLASSIFIED SAI-79-748-WA NL

2 OF 2
ADA
067510

END
DATE
FILMED
6-79
DDC

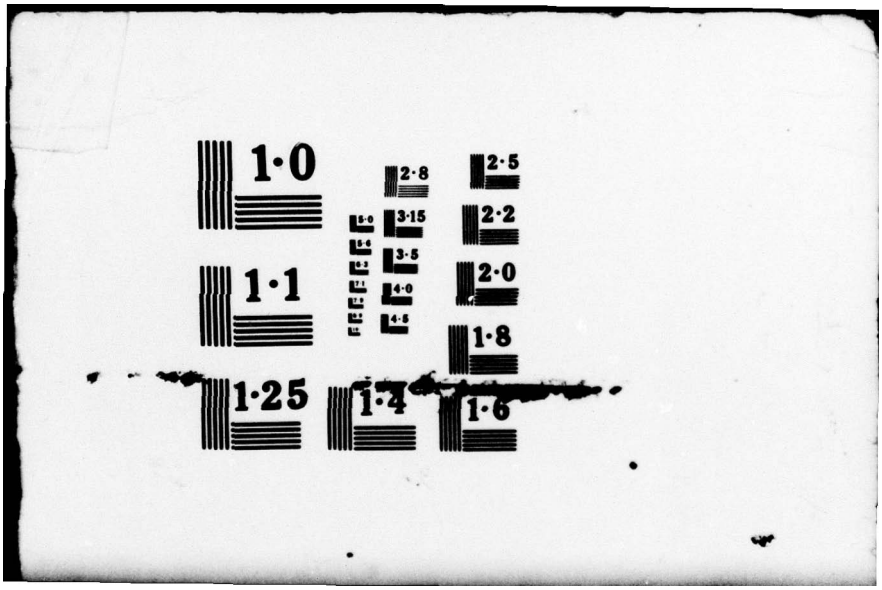
1·0
1·1
1·25
1·4
1·6
1·8
2·0
2·2
2·5
2·8
3·15
3·5
4·0

9. Clancy, R.M., 1977, "The Effect of Ocean Thermal Power Plants on the Thermodynamic Characteristics of the Marine Atmosphere: Some Preliminary Results from a One-Dimensional Model", presented at OTEC Workshop on Environmental Effects, June 1977, Cape Canaveral, FL., 22 pp.

10. Clarke, R.H., 1970, "Recommended Methods for the Treatment of the Boundary Layer in Numerical Prediction Models", Mon. Wea. Rev., 97, 77-85.

11. Deardorff, J.W., G.E. Willis and D.K. Lilly, 1969, "Laboratory Investigation of Non-Steady Penetrative Convection", J. Fluid Mech., 35, 7-31.

12. Danard, M.B., 1969, "A Simple Method of Including Longwave Radiation in a Tropospheric Numerical Prediction Model", Mon. Wea. Rev., 97, 77-85.

13. Dunckel, M., L. Hasse, L. Krugermeyer, D. Schriever and J. Wucknitz, 1974, "Turbulent Fluxes of Momentum, Heat, and Water Vapor in the Atmospheric Surface Layer at Sea during ATEX", Boundary-Layer Meteorol., 6, 81-106.

14. Elsasser, W.M., 1960, Meteorol. Monographs, 4 (23), 43 pp.

15. Esbensen, S., 1975, "An Analysis of Subcloud-Layer Heat and Moisture Budgets in the Western Atlantic Trades", J. Atmos. Sci., 32, 1921-1933.

16. Garstang, M. and A.K. Betts, 1974, "A Review of the Tropical Boundary Layer and Cumulus Convection: Structure, Parameterization and Modeling", Bull. Amer. Meteorol. Soc., 55, 1195-1205.

17. Haltiner, G.J., 1971, Numerical Weather Prediction, John Wiley and Sons, Inc., New York, 317 pp.

18. Högstrom, U., 1974, "A Field Study of the Turbulent Fluxes of Heat, Water Vapor and Momentum at a 'Typical' Agricultural Site", Quart. J. Roy. Meteorol. Soc., 100, 624-639.

19. Hsu, S.A., 1974, "On the Log-Linear Wind Profile and the Relationship Between Shear Stress and Stability Characteristics over the Sea", Boundary-Layer Meteorol., 6, 509-514.

20. Kraus, E.B., 1972, Atmosphere-Ocean Interaction, Clarendon Press, 275 pp.

21. Kraus, E.B., 1977, "Ocean Surface Drift Velocities", J. Phy. Oceanogr., 7, 606-609.

22. Lee, J.D., 1973, "Numerical Simulation of the Planetary Boundary Layer over Barbedos, W. I.", Ph.D. Dissertation, The Florida State University, Tallahassee.

23. Lemone, M.A. and W.T. Pennell, 1976, "The Relationship of Trade Wind Cumulus Distribution to Subcloud Layer Fluxes and Structure", Mon. Wea. Rev.

24. Lilly, D.K., 1968, "Models of Cloud-Topped Mixed Layers under a Strong Inversion", Quart. J. Roy. Meteorol. Soc., 94, 292-309.

25. Malkus, J.S., 1958, "On the Structure of the Trade Wind Moist Layer", Papers Phys. Oceanogr. Meteor., 13, No. 2, 47 pp.

26. Nitta, T., 1975, "Observational Determination of Cloud Mass Flux Distributions", J. Atmos. Sci., 32, 73-91.

27. Ogura, Y. and H-R Cho, 1973, "Diagnostic Determination of Cumulus Cloud Populations from Observed Large-Scale Variables", J. Atmos. Sci., 30, 1276-1286.

28. Ogura, Y. and H-R Cho, 1974, "On the Interaction Between the Subcloud and Cloud Layers in Tropical Regions", J. Atmos. Sci., 31, 1850-1859.

29. O'Brien, J.J., 1970, "A Note on the Vertical Structure of the Eddy Exchange Coefficient in the Planetary Boundary Layer", J. Atmos. Sci., 27, 1213-1215.

30. Pennell, W.T. and M.A. Lemone, 1974, "An Experimental Study of Turbulence Structure in the Fair-Weather Trade Wind Boundary Layer", J. Atmos. Sci., 31, 1308-1323.

31. Paulson, C., 1970, "The Mathematical Representation of Wind Speed and Temperature Profiles in the Unstable Atmospheric Surface Layer", J. Appl. Meteor., 9, 857-861.

32. Pielke, R.A., 1974, "A Three-Dimensional Model of the Sea Breezes over South Florida", Mon. Wea. Rev., 102, 115-139.

33. Piacsek, S., P. Martin, J. Toomre and G. Roberts, 1976, "Recirculation and Thermocline Perturbations from Ocean Thermal Power Plants", NRL-GFD/OTEC 2-76, 25 pp.

34. Pond, S., 1971, "Air-Sea Interaction", Trans. Amer. Geophys. Union (IUGG, 52, 389-394.

35. Pond, S., 1972, "The Exchange of Momentum, Heat and Moisture at the Ocean-Atmosphere Interface", Proceedings of a Symposium on Numerical Models of Ocean Circulations, Washington, D.C., Oct. 1972, ed. N. H. Durham, U.S. National Acad. Sciences, Washington, D.C., 26-36.

36. Pond, S., D.B. Fissel and C.A. Paulson, 1974, "A Note on Bulk Aerodynamic Coefficients for Sensible Heat and Moisture Fluxes", Boundary-Layer Meteorol., 6, 333-339.

37. Randall, D. and A. Arakawa, 1978, "A Parameterization of the Planetary Boundary Layer for Numerical Models of the Atmosphere", to be published.

38. Reed, R.K., 1976, "On Estimation of Net Long-Wave Radiation from Oceans", J. Geophys. Res., 81, 5793-5794.

39. Roll, H.U., 1965, Physics of the Marine Atmosphere, Academic Press, 426 pp.

40. Schubert, W.H., 1973, "The Interaction of a Cumulus Cloud Ensemble with the Large-Scale Environment", Ph.D. Dissertation, University of California, Los Angeles.

41. Schubert, W.H., 1974, "Cumulus Parameterization Theory in Terms of Feedback and Control", Atm. Sci. Paper No. 226, US ISSN 0067-0340, Dept. of Atmospheric Science, Colorado State University, Fort Collins, Colorado, 19 pp.

42. Schubert, W.H., 1976, "Experiments with Lilly's Cloud-Topped Mixed Layer Model", J. Atmos. Sci., 33, 436-445.

43. Shukla, J., 1975, "Effect of an Arabian Sea Surface Temperature Anomaly on the Indian Summer Monsoon: A Numerical Experiment with the GFDL Model", J. Atmos. Sci., 32, 503-511.

44. Shukla, J. and B.M. Misra, 1977, "Relationships Between Sea Surface Temperature and Wind Speed over the Central Arabian Sea, and Monsoon Rainfall over India", Mon. Wea. Rev., 105, 998-1002.

45. Simpson, J., 1971, "On Cumulus Entrainment and One-Dimensional Models", J. Atmos. Sci., 28, 449-455.

46. Sommeria, G., 1976, "Three-Dimensional Simulation of Turbulent Processes in an Undisturbed Trade Wind Boundary Layer", J. Atmos. Sci., 33, 216-241.

47. Soong, S-T. and Y. Ogura, 1976, "A Determination of the Trade Wind Cumuli Population using BOMEX Data and an Axisymmetric Cloud Model", J. Atmos. Sci., 33, 992-1007.

48. Washington, W. and A. Kasahara, 1970, "A January Simulation with the Two-Layer Version of the NCAR General Circulation Model", Mon. Wea. Rev., 98, 559-580.

49. Wendland, W.M., 1977, "Tropical Storm Frequencies Related to Sea Surface Temperatures", J. Appl. Meteor., 16, 477-481.

50. Yanai, M., S. Esbensen and J-H Chu, 1973, "Determination of Bulk Properties of Tropical Cloud Clusters from Large-Scale Heat and Moisture Budgets", J. Atmos. Sci., 30, 611-627.